Published online 20 August 2021

Nucleic Acids Research, 2021, Vol. 49, No. 20 ***e116***
https://doi.org/10.1093/nar/gkab714

m^{6}A-express: uncovering complex and condition-specific m^{6}A regulation of gene expression

Teng Zhang [1], Shao-Wu Zhang [1,*], Song-Yao Zhang[1], Shou-Jiang Gao [2], Yidong Chen[3,*] and Yufei Huang[4,*]

[1]Key Laboratory of Information Fusion Technology of Ministry of Education, School of Automation, Northwestern Polytechnical University, Xi'an, 710027 Shaanxi, China, [2]UPMC Hillman Cancer Center, Department of Microbiology and Molecular Genetics, University of Pittsburgh, Pittsburgh, Pennsylvania, PA 15232, USA, [3]Department of Populational Health Science, University of Texas Health San Antonio, San Antonio, TX 78229, USA and [4]UPMC Hillman Cancer Center, Department of Medicine, School of Medicine, University of Pittsburgh, Pittsburgh, Pennsylvania, PA 15232, USA

Received February 26, 2021; Revised July 06, 2021; Editorial Decision August 03, 2021; Accepted August 17, 2021

ABSTRACT

N^6-methyladenosine (m^{6}A) is the most abundant form of mRNA modification and controls many aspects of RNA metabolism including gene expression. However, the mechanisms by which m^{6}A regulates cell- and condition-specific gene expression are still poorly understood, partly due to a lack of tools capable of identifying m^{6}A sites that regulate gene expression under different conditions. Here we develop *m^{6}A-express,* the first algorithm for predicting condition-specific m^{6}A regulation of gene expression (m^{6}A-reg-exp) from limited methylated RNA immunoprecipitation sequencing (MeRIP-seq) data. Comprehensive evaluations of *m^{6}A-express* using simulated and real data demonstrated its high prediction specificity and sensitivity. When only a few MeRIP-seq samples may be available for the cellular or treatment conditions, *m^{6}A-express* is particularly more robust than the log-linear model. Using *m^{6}A-express*, we reported that m^{6}A writers, METTL3 and METTL14, competitively regulate the transcriptional processes by mediating m^{6}A-reg-exp of different genes in Hela cells. In contrast, METTL3 induces different m^{6}A-reg-exp of a distinct group of genes in HepG2 cells to regulate protein functions and stress-related processes. We further uncovered unique m^{6}A-reg-exp patterns in human brain and intestine tissues, which are enriched in organ-specific processes. This study demonstrates the effectiveness of *m^{6}A-express* in predicting condition-specific m^{6}A-reg-exp and highlights the complex, condition-specific nature of m^{6}A-regulation of gene expression.

INTRODUCTION

N^6-methyladenosine (m^{6}A) is the most abundant methylation in mRNA, found in >25% mRNAs in mammalian cells and forms an important regulatory circuitry that controls many aspects of RNA metabolism (1–8). It is enriched in regions close to the stop codon with a consensus RRACH motif (R = G or A; H = A, C, or U) (9). Unlike DNA methylation, m^{6}A is highly dynamic (10); it is catalyzed by 'writers' or m^{6}A methylases, including METTL3 and METTL14 (11), and can be removed by 'erasers' such as ALKBH5 (12) and m6A demethylases (FTO) (10). m^{6}A has been shown to influence diverse cellular and biological processes including dopaminergic midbrain circuity (13), circadian period (6,14), fertility (7,14) and sex determination (15,16), development (1,2,14), cell reprogramming (17–19) and meiosis (20). Evidence of m^{6}A's involvement in different diseases, especially cancer, is accumulating. FTO is shown to promote leukemic cellular transformation and leukemogenesis (14,21). The breast cancer stem cell phenotype is induced by hypoxia in an ALKBH5-dependent manner, and knockdown of ALKBH5 in MDA-MB-231 breast cancer cells significantly reduces their capacity for tumor initiation (22,23). METTL3 promotes growth, survival and invasion of human lung cancer cells by facilitating the translation initiation of certain cancer mRNAs (24). METTL14 and ALKBH5 form a positive feedback loop to regulate breast cancer growth and invasion (25). Also, m^{6}A is found to be involved in viral infection of HIV (26,27), hepatitis C virus (28), Zika virus (29) and Kaposi's sarcoma-associated herpesvirus (KSHV) (30,31). While m^{6}A's close involvement in

*To whom correspondence should be addressed. Tel: +86 029 88431308; Fax: +86 029 88431306; Email: zhangsw@nwpu.edu.cn
Correspondence may also be addressed to Yidong Chen. Tel: +1 210 562 9163; Fax: +1 210 562 9163; Email: cheny8@uthscsa.edu
Correspondence may also be addressed to Yufei Huang. Tel: +1 412 623 2617; Email: yuh119@pitt.edu

many processes and diseases is clear, specific mechanisms by which m^{6}A regulates downstream processes and phenotypes in different conditions are still elusive.

Under different conditions, m^{6}A can mediate different stages of mRNA metabolism including translation, nuclear export, splicing and mRNA degradation (32) by recruiting different 'reader' proteins including YTH family proteins and their cofactor RNA-binding proteins (RBPs). Among many processing stages controlled by m^{6}A, the primary mode of m^{6}A post-transcription regulation is mRNA stability regulation. While all YTHDF1-3 selectively bind to m^{6}A sites to promote mRNA decay (33), YTHDF2 has the strongest affinity to degrade the targeted mRNAs (34). In contrast, readers IGF2BP1-3 stabilizes mRNA by interacting with cofactors HuR and MATR3 (35). These readers recognize distinct m^{6}A sites in CDS and 3'UTR and exhibit condition-specific binding density (35). Here, we refer to condition-specificity as either the specific cell conditions such as stress and viral infection or different cell types. This m^{6}A regulation of gene expression is also highly condition-specific, partly due to the dynamic expressions under different cell types, cell conditions and divergent cellular localization of m^{6}A effectors (writers, erasers and readers). This condition-specific regulation provides the unique ability for m^{6}A to tune gene expressions. However, the highly dynamic nature of m^{6}A regulation of gene expression complicates our understanding of the mechanisms by which m^{6}A regulates its downstream functions.

The widespread adoption of high-throughput m^{6}A profiling methods, especially methylated RNA immunoprecipitation sequencing, or MeRIP-seq (9,36) and rapid advances in machine learning provide an opportunity to computationally predict condition-specific m^{6}A regulation of gene expression (m^{6}A-reg-exp). There is a large collection of algorithms devoted to predicting m^{6}A sites from mRNA sequences (37–43). They are useful in assessing condition-independent methylation potentials of a candidate site, but they nevertheless do not inform condition-specific m^{6}A modifications. Informatics tools for MeRIP-seq-based m^{6}A peak detection [*exomePeak* (44,45), *MeTPeak* (46) and *deep-m^{6}A* (47)], differential m^{6}A analysis [*exomePeak, MeTDiff* (48), *QNB* (49) and *RADAR* (50)] and visualization [*Guitar* (51)] have also been developed. They, particularly *exomePeak*, are now widely adopted to identify condition-specific m^{6}A methylations in many studies (35,52–58). As the focus of m^{6}A research shifts from discovery to functional studies, computational tools that facilitate the prediction of m^{6}A functions have also emerged. *m^{6}A-Driver* (59), *hot-m^{6}A* (47) and *FunDMDeep-m^{6}A* (60) were developed to predict m^{6}A driver genes and networks from MeRIP-seq. Both *hot-m^{6}A* and *DRUM* (61) are tools for predicting m^{6}A disease associations. A co-methylation network approach was also established in (62) and identified a set of cell-specific m^{6}A co-regulating RBPs. However, none of these tools can be used to infer condition-specific m^{6}A-reg-exp.

In this paper, we developed *m^{6}A-express,* the first tool for predicting condition-specific m^{6}A-reg-exp from MeRIP-seq (See Supplementary Table S1 for comparison with other tools). *m^{6}A-express* is based on a log-linear relationship between m^{6}A intensity and gene expression, found enriched in genes harboring m^{6}A sites that regulate gene expression. However, a common challenge in studying condition-specific m^{6}A regulatory functions is the limited MeRIP-seq replicates. To combat this limitation and enable robust prediction, *m^{6}A-express* adopts a hierarchical Bayesian formulation. We comprehensively validated *m^{6}A-express*'s performance using both simulated and real MeRIP-seq datasets. We showed that *m^{6}A-express* significantly improved the robustness of predicting m^{6}A-reg-exp and estimating the regulation strength over the commonly used log-linear model under small samples and other experimental settings, and it achieved higher prediction specificity, precision and sensitivity. We applied *m^{6}A-express* to predict METTL3- and METTL14-mediated m^{6}A-reg-exp in HeLa cells and revealed a competitive transcription regulation. Comparing METTL3-mediated m^{6}A-reg-exp between Hela and HepG2 cells, we observed a distinct condition-specific (or cell-specific) m^{6}A regulation with distinct gene sets and regulation functions. We further applied *m^{6}A-express* to MeRIP-seq samples of human brain and intestine tissues and observed clear condition-specific (or organ-specific) m^{6}A-reg-exp that involved in distinct, organ-related functional pathways. Taken together, *m^{6}A-express* is a powerful data-driven, hypothesis-generating tool that can accelerate the investigation of the mechanistic roles of m^{6}A in mediating gene expression and downstream biological processes.

MATERIALS AND METHODS

Overview of the *m^{6}A-express* framework

We consider a scenario where transcriptome-wide m^{6}A under different conditions (treated/disease versus control; different tissues/infection stages) are profiled by MeRIP-seq. Note that *m^{6}A-express* is not restricted to MeRIP-seq but can be applied to any high-throughput methods such as MAZTER-seq or nanopore sequencing (63,64) that quantify m^{6}A stoichiometry. We assume that for an m^{6}A site that regulates mRNA expression, the change of its m^{6}A level is predictive of the change in the expression level of the methylated gene, where the m^{6}A level is quantified by MeRIP-seq IP reads and the expression is measured by MeRIP-seq Input reads. *m^{6}A-express* is an algorithm designed to assess the degree to which such a predictive relationship exists between m^{6}A levels and gene expressions for the specific conditions under consideration.

Before applying *m^{6}A-express*, m^{6}A peaks are first identified from each MeRIP-seq sample using *exomePeak* (Figure 1 and Supplementary Figure S1). The m^{6}A intensity for each gene that harbors m^{6}A peaks is computed (Peak Calling and Quantifying Subsection; Supplementary Figure S1). We then select candidate genes based on the following criteria: when two conditions (treated versus control) are considered, candidate genes are differential expression genes that harbor differential m^{6}A peaks (or DE-DM genes); otherwise, when there are more than two conditions (multiple tissue types or time points), candidate genes are those that contain highly variable m^{6}A peaks (Supplementary Figure S1). Afterward, m6A-*express* is applied to all the candidate genes. *m^{6}A-express* uses a negative binomial regression model to assess the regulatory impact of m^{6}A

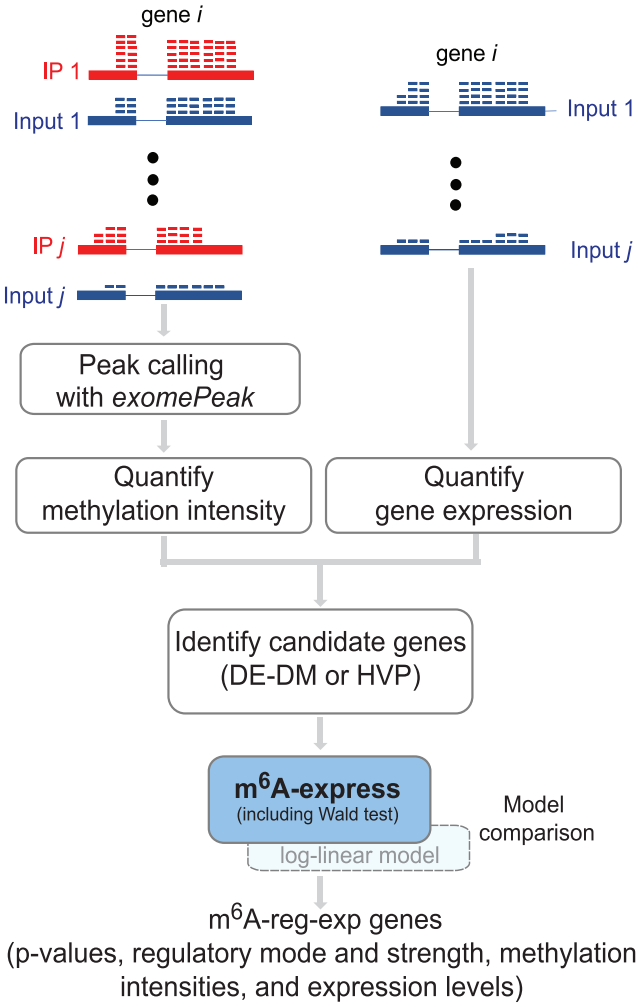

Figure 1. Overview of *m6A-express* prediction pipeline.

intensity (MeRIP-seq IP) on the expression level (MeRIP-seq Input) for each candidate gene. A key model parameter β_1 represents the mode (positive or negative) and the strength of the m^{6}A regulation of gene expression. Once the model parameters are inferred, the Wald test is used to test if the m^{6}A intensity of a candidate gene could regulate its gene expression. The candidate genes test significant for FDR < 0.05 by the Wald test are termed m^{6}A-reg-exp genes, whose m^{6}A intensities are predicted to regulate their gene expressions. Among the outputs of *m6A-express* are a list of m^{6}A-reg-exp genes, their associated regulatory mode and strength (β_1), the methylation intensities and the gene expression levels. *m6A-express* is implemented as a python/R package and is freely available at https://github.com/Yufei-Huang-Lab/m6Aexpress.

Sample normalization

INPUT and IP samples were normalized to reduce the bias such as outliers, sequencing library size variations and sample-wise IP efficiency difference. For the INPUT sample normalization, we adopted the median-of-ratio method for INPUT sample normalization; this method is similar to the size factor normalization in *DESeq* (65), which was shown to be robust against gene expression outliers. For the IP samples, to reduce the bias from sequence depth and overall IP efficiency, all the peaks' reads count was first summed up to obtain an IP library size. Then, the median-of-ratio method was applied for IP sample normalization.

Peak calling and quantifying the methylation intensity

For concerned conditions, m^{6}A peaks were called from all the replicates using the *exomePeak* R package (44). Then, the methylation intensity of the k-th peak of gene i in sample j, M_{kij}, was computed as the log of the normalized IP read counts divided by the normalized INPUT read counts

$$M_{kij} = log_2\left(\frac{C_{IP,kij}/S_{IP,j}}{C_{INPUT,kij}/S_{INPUT,j}}\right)$$

where $C_{IP,kij}$ and $C_{INPUT,kij}$ are the read counts of in the paired IP and INPUT sample, respectively, and $S_{IP,j}$ and $S_{INPUT,j}$ are the sample size factors for the paired IP and INPUT sample obtained during normalization, respectively. The effective methylation intensity x_{ij} for gene i in sample j is then computed as the weighted average of the peak intensities, i.e.,

$$x_{ij} = \frac{\sum_{k=1}^{K} x_{kij}}{K}, \quad x_{kij} = M_{kij}\, e^{-(d_{ki}/d_0)}$$

where K is the number of peaks in gene i, M_{kij} is the methylation intensity of peak k, d_{ki} is the distance between the center of peak k, and the stop codon and d_0 is a decay coefficient, set by default as the 75% quantile of all distances between the peaks and their corresponding stop codon (Supplementary Figure S3) but can be defined by the user. The exponential term in x_{kij} models two factors: (i) m^{6}A sites that regulate mRNA stability are enriched near the stop codon (34), and (ii) the regulatory effect of m^{6}A intensity is scaled down for peaks away from the stop codon.

Quantifying gene expression and differential expression

The gene expression was quantified by the reads count from INPUT data using *featureCounts* function, which is part of R/Bioconductor package *Rsubread* (66) under the default setting. Differential expression analysis was performed using *DEseq2* (67) (R/Bioconductor), and significant differentially expressed genes (DEGs) were selected with FDR $<$ 0.05.

Identifying candidate genes

For the treated versus control cases, the candidate genes are differentially expressed genes with differential m^{6}A peaks. Differential m^{6}A peaks were identified by *QNB* (49) under the default setting as the peaks showing significant differences in peak fold enrichment with P-value < 0.05. For cases with multiple sub-conditions (i.e. different time-points or different tissues), the candidate genes are those containing highly variable peaks (HVPs), which were defined as peaks having a high coefficient of variations (CVs), or CVs > 0.3 as suggested in (62) and demonstrated in Supplementary Figure S4, where CV was computed as the standard

deviation of the methylation intensity divided by the mean of the methylation intensity across samples from multiple conditions.

The m^{6}A-express model and predicting m^{6}A-reg-exp genes

The log-linear relationship between gene expression and m^{6}A intensity. To investigate the relationship between m^{6}A level and gene expression, we predicted the m^{6}A peaks using *exomePeak* in the MeRIP-seq dataset of METTL3 knockdown (KD, $n_1 = 2$) and wildtype (WT, $n_2 = 2$) HeLa cells (GSE46705). We first inspected FOXM1 and CREBBP, two cancer target genes whose mRNA stability was shown to be regulated by m^{6}A in cancer (34,68). We found that their normalized gene expression could be regressed by the intensities of their associated m^{6}A peaks by a log-linear model (Supplementary Figure S5). To verify this relationship at a larger scale, we consulted the mRNA lifetime data of METTL3 KD and WT HeLa cells (GSE98856). Because m^{6}A induces mRNA decay, METTL3 KD would increase lifetime among its target mRNAs (69), thus influencing a change in gene expression. We identified 258 genes whose mRNA lifetime increased and significantly upregulated after METTL3 KD (FDR < 0.05); these genes are high confidence candidates for genes whose mRNA stability is regulated by m^{6}A. Furthermore, we found that among the genes whose m^{6}A levels regulate their mRNA stability, those whose normalized gene expressions could be regressed by their m^{6}A intensities with a log-linear model are significantly enriched (P-value $= 7.56 \times 10^{-16}$; odds ratio $=$ 34.2; Fisher's exact test; Supplementary Table S2).

The hierarchical Bayesian negative binomial (NB) regression model for limited samples. However, due to limited MeRIP-seq replicates used in most studies (often as few as two or three replicates per condition), the conventional log-linear model lacks the power and sensitivity to predict m^{6}A-reg-exp. To address this limitation, *m^{6}A-express* employs a Bayesian negative binomial (NB) regression model to model the relationship between the read count (expression level) y_{ij} and m^{6}A intensity x_{ij} of a candidate gene i in sample j

$$y_{ij} \sim NB\left(S_j\mu_{ij},\ \alpha_i\right);\quad log\ \left(\mu_{ij}\right) = \beta_{i0} + \beta_{i1}x_{ij} \quad (1)$$

where S_j is the sample size-factor of the INPUT sample obtained from the normalization process, α_i is the dispersion parameter of gene i, μ_{ij} is the normalized expression of gene i in sample j, which is modeled as a log-linear function of x_{ij} in Equation (1), with the parameters β_{i0} modeling the baseline log gene expression and β_{i1}, the key parameter, denoting the mode (positive or negative) and degree of influence of m^{6}A methylation on gene expression. To enable robust estimation of model parameters with limited samples, *m^{6}A-express* implements a hierarchical Bayesian strategy (Supplementary Figure S2) to imposes a set of prior distributions on β_{i1} and other model parameters, which are shared across genes. The shared prior model distributions allow *m^{6}A-express* to pool information across genes to improve individual genes' prediction power and robustness over the log-linear model that separately considers each gene's prediction. More details on the model inference and m^{6}A-reg-exp gene prediction are given in Supplementary Methods, where maximum *a posteriori* (MAP) estimates of model parameters (β_{i0}, β_{i1}) are derived [Supplementary Methods, Equation (10)] and obtained using a custom implemented empirical Bayes method.

Predicting m^{6}A-reg-exp genes and assessing the significance. Because $\beta_{i1} = 0$ would suggest that m^{6}A has no impact on the expression of gene i, once the model parameters are inferred, the Wald test is applied to test whether a candidate gene i is an m^{6}A-reg-exp gene by

$$H_0:\ \beta_{i1} = 0 \text{ vs. } H_1:\ \beta_{i1} \neq 0.$$

The Benjamini-Hochberg (BH) (70) procedure will be applied to obtain the FDR value for each gene, and m^{6}A-reg-exp genes will be selected by FDR < 0.05.

The simulated datasets

To evaluate the performance of *m^{6}A-express* and assess the impact of experimental factors on the inference and prediction performance, we applied *m^{6}A-express* to the simulated datasets of two conditions. The simulated datasets include paired gene expression level and methylation intensity (both in read count unit) for genes under two conditions. To mimic the real scenarios, we utilized the MeRIP-seq dataset of METTL3 knockout (KD) and wild-type (WT) HeLa cells (M3-KD-HeLa; GSE46705) to build our simulation of read counts and methylation intensities for replicates of each condition. We first applied the QNB package (49) to detect the differential peaks in METTL3 KD versus WT conditions. For genes containing these differential m^{6}A peaks, we used DEseq2 to assess their differential expression. The genes significantly differentially expressed (FDR < 0.05) and differentially methylated (DE-DM) were selected as candidate genes.

We further assumed the methylation intensity x_{ij} of gene i in sample $j$following a Gaussian distribution, i.e. $x_{ij} \sim \mathcal{N}(\bar{x}_i,\ {\sigma_i}^2)$ and we used methylation intensities of the candidate genes to estimate the parameters $\bar{x}_i$ and ${\sigma_i}^2$ for each gene i (Supplementary Methods S1.4 and Supplementary Figure S6). Using $\bar{x}_i$ and ${\sigma_i}^2$, we simulated methylation intensity for the Gaussian distribution for each gene in each replicate under two conditions. Next, given the read count of the INPUT samples and methylation intensity of these DE-DM genes, we fitted the log-linear model to estimate the regression coefficients β_{i0} and β_{i1} for each gene separately (Supplementary Methods S1.5 and Supplementary Figure S7). To assess the impact of different m^{6}A regulation levels on m^{6}A-express performance, we stratified the regulation levels based on the empirical distribution of β_{i1} into three categories, i.e. weak ($\mu_{\beta_1} = -0.3$), medium ($\mu_{\beta_1} = -0.6$) and strong ($\mu_{\beta_1} = -1.28$) regulatory strength (Supplementary Methods S1.5). We estimated hyper-parameters of the normal prior of β_{i0} and β_{i1} for three different regulation levels based on the destructions of β_{i0} and β_{i1} estimated from the real data. Then, for a given regulation level, the coefficients β_{i0} and β_{i1} for gene i were simulated from their corresponding normal priors β_{i1} (Supplementary Methods S1.5). We simulated both genes whose expression is regulated by

m^{6}A or m^{6}A-reg-exp genes and those with no regulation or non-m^{6}A-reg-exp genes. When simulating non-m^{6}A-reg-exp genes, we set $\beta_{i1} = 0$.

After generating the methylation intensity x_{ij} and regression coefficients β_{i0} and β_{i1} for each gene, the normalized expected gene expression μ_{ij} and dispersion α_i were calculated and the read count y_{ij} of gene i in jth sample was simulated from the negative binomial distribution (Supplementary Methods S1.6).

Identifying genes with increased RNA half-life

The mRNA lifetime data of METTL3 KD versus Control and YTHDF2 versus Control were processed according to the pipeline in (69). Briefly, for each gene, the RNA-degradation rate was determined as the $\log_2$ fold-change in RNA abundance (quantified by RPKM) at 3 or 6 h versus 0 h after transcription inhibited. Then, the average degradation rate of 3 and 6 h was used to calculate the RNA half-life per gene in each condition (METTL3/YTHDF2 KD or Control). The fold-change of RNA half-life between two conditions (e.g. METTL3 KD versus Control) were used to quantify the difference of RNA half-life. We determined the genes with consistent fold-change > 1.1 in single (for METLL3 KD) or two replicates (for YTHDF2 KD) as those with increased half-life.

Identifying YTHDF2 binding clusters

YTHDF2 binding clusters were identified from PAR-CLIP-seq data (GSE49339) by PARalyzerV1.1 with default settings (71).

MeRIP-seq datasets

We selected three case studies to assess *m^{6}A-express* predictions. The first two examines METLL3/METTL14-mediated m^{6}A-reg-exp in cancer cell lines and the last study investigates global m^{6}A-reg-exp in human brain and intestine tissues. They are summarized as follows.

MeRIP-seq data from human cancer cell lines. The MeRIP-seq dataset from the HeLa cell line (GSE46705) includes two replicates of IP and INPUT samples from METLL3 KD, METTL14 KD and WT HeLa cells. The second dataset derived from the HepG2 cell line (GSE102620) consists of two replicates of IP and INPUT samples from METTL3 KD and WT HepG2 cells. Raw sequence data from both datasets were download from the Sequence Read Archive (SRA, NCBI) and corresponding metadata from the Gene Expression Omnibus (GEO, NCBI).

MeRIP-seq data from the human brain and intestine tissue. The MeRIP-seq samples from different human brain and intestine tissues (CRA001315) were collected from the Genome Data Archive (China National Center for Bioinformation) (72). The brain tissue samples ($N = 6$) include one sample each from the hypothalamus and brainstem (from donor #5), two cerebellum samples (from donors #5 and #6) and two cerebrum samples (from donors #5 and #7). The intestine tissue samples ($N = 8$) include two duodenum samples (donors #5 and #3), two jejunum samples (from donors #4 and #5), two appendix samples (from donors #3 and #5) and two rectum samples (from donors #4 and #5).

mRNA lifetime and YTHDF2 PAR-CLIP-seq datasets

mRNA lifetime data from HeLa cells include one set of METTL3 KD versus Control (GSE98856) and two replicates of YTHDF2 KD versus Control (GSE49339). YTHDF2 PAR-CLIP-seq data from HeLa cells (GSE49339) include three replicates with overexpression of flag-tagged YTHDF2. Raw data were downloaded SRA and corresponding metadata from the GEO.

RESULTS

Performance of *m^{6}A-express*

m^{6}A-express *is robust against the regulation strength, number of m^{6}A-reg-exp genes and small number of replicates.* We first assessed the impact of experimental factors on the inference and prediction performance of *m^{6}A-express* using the simulated datasets. We first investigated the estimation of regulatory strength, β_1, from the data generated based on different regulatory strengths (weak, medium and strong) and different sample replicates (two, three and four) where we simulated 2000 m^{6}A-reg-exp genes for each experimental condition. We compared the normalized root mean square errors (NRMSEs) of estimated β_1 from *m^{6}A-express* and the conventional log-linear model. *m^{6}A-express* obtained much smaller NRSMEs for all these different experimental conditions and the improvement is especially pronounced for estimating weak regulations with fewer replicates (Figure 2A and Supplementary Table S3). For two replicates with the weak strength, *m^{6}A-express* achieved >12-fold reduction in NRMSE compared with the log-linear [0.3492 ± 0.0118 (*m^{6}A-express*) versus 4.4849 ± 0.4378 (log-linear)]. Also, for the log-linear, we observed that NRMSEs drop quickly with more replicates or regulation strength. In contrast, thanks to the hierarchical Bayesian model, *m^{6}A-express* maintained low NRMSEs across different regulatory strengths and sample replicates with much smaller standard deviations in NRMSEs. We further evaluated the impact of the number of m^{6}A-reg-exp genes on the estimation of β_1. We simulated three replicate data sets generated from 600, 800 and 1200 m^{6}A-reg-exp genes with different regulatory strengths. We noticed that the number of m^{6}A-reg-exp genes had little impact on *m^{6}A-express* and log-linear model's performance, but the log-linear model has higher NRSME and variation than *m^{6}A-express* (Figure 2B). Taken together, these results demonstrate that *m^{6}A-express* has a much better performance for estimating β_1 than that from the log-linear model, and its performance is also more robust than the log-linear model against the regulation strength, replicates and the number m^{6}A-reg-exp genes.

We then evaluated the performance of *m^{6}A-express* for detecting m^{6}A-reg-exp genes (Figure 2C). Again, we first tested for the different number of replicates and regulatory

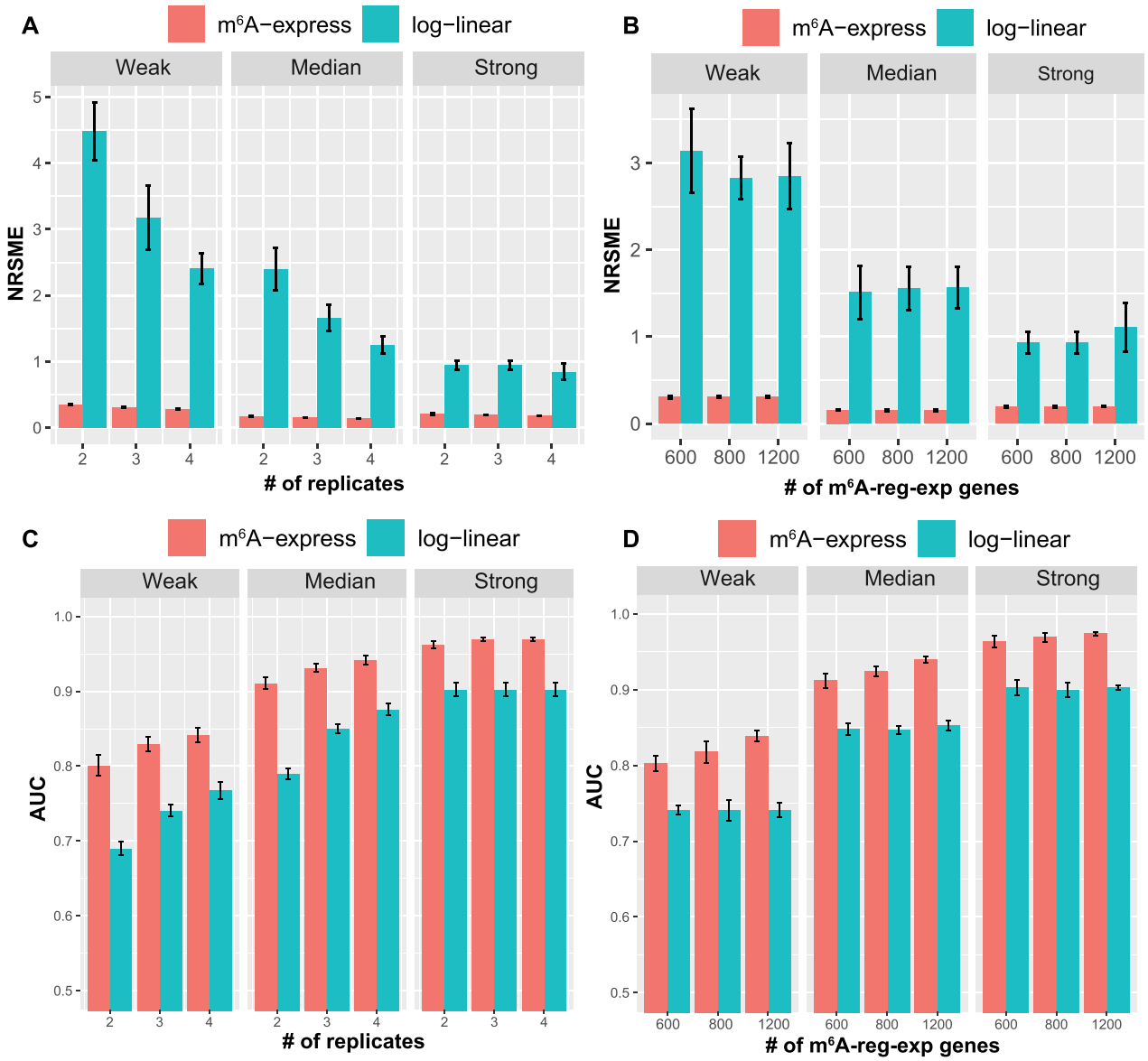

Figure 2. Performance of *m⁶A-express* and the log-linear evaluated using the simulation data. (**A**) Normalized root-mean-square error (NRMSE) of estimating β_1 for different regulatory strengths with different replicates. (**B**) NRMSE of estimating β_1 for different numbers of simulated m^{6}A-reg-exp genes with three replicates. (**C**) AUCs of detecting m^{6}A-reg-exp genes under different regulatory strengths with different replicates. (**D**) AUCs of detecting m^{6}A-reg-exp genes for different numbers of simulated m^{6}A-reg-exp genes under different regulatory strengths with three replicates.

strengths. For each condition, we simulated 1000 m^{6}A-reg-exp genes and 1000 non-m^{6}A-reg-exp genes ($\beta_1 = 0$). We applied both *m⁶A-express* and the log-linear model to estimate the regulation coefficient β_1 of these 2000 genes and predicted m^{6}A-reg-exp genes. We used the area under the receiver operating characteristic curve (AUC) to measure the prediction performance. Similar to the results for β_1 estimation, *m⁶A-express* significantly outperformed the log-linear model for all regulation strengths (Figure 2C and Supplementary Table S4). We observed that with only two replicates, *m⁶A-express* could achieve 91.08% and 96.25% AUC for the medium and strong strength (Supplementary Table S4). Specifically, m6A-*express* achieved the highest AUC improvements (11% AUC for the weak and 12% AUC for the medium strength) over the log-linear model for two replicates. Even though the improvement tapered with the increase of replicates and regulatory strength, *m⁶A-express* still reported ∼6% improvement for four replicates under the strong the weak strength. We further investigated the influence of different numbers of m^{6}A-reg-exp genes (600, 800 or 1200 m^{6}A-reg-exp genes out of 2000 simulated genes) on the predictive power of *m⁶A-express* under three regulatory strengths (Figure 2D and Supplementary Table S5). Again, both *m⁶A-express* and the log-linear model's AUCs increased with higher regulatory strength with *m⁶A-express* achieved 6–8% AUC improvement over the log-linear. Due

mainly to the hierarchical Bayesian model, the performance of *m⁶A-express* especially improved with a higher number of m⁶A-reg-exp genes at weak and medium regulatory strength. In contrast, the number of regulatory genes has no impact on the performance of the log-linear model. Collectively, our results show that *m⁶A-express* has robust performance under different regulatory strengths and sample sizes.

m⁶A-express *produces higher specificity, precision and sensitivity in real MeRIP-seq data.* We further assessed the performance for *m⁶A-express* using three real MeRIP-seq datasets: METTL3 KD and WT HeLa cells (M3-KD-HeLa; GSE46705, $n = 4$), METTL14 KD and WT HeLa cells (M14-KD-HeLa; GSE46705, $n = 4$), and METTL3 KD and WT HepG2 cells (M3-KD-HepG2; GSE102620, $n = 4$). For each dataset, we first detected 1401 (in M3-KD-HeLa), 900 (in M14-KD-HeLa) and 433 (in M3-KD-HepG2) DE-DM candidate genes, which were subject to the prediction of m⁶A-reg-exp by *m⁶A-express* and the log-linear model. To evaluate the specificity of the two models, we adopted a similar strategy as (50): gene expression read counts and methylation intensities were randomly shuffled separately (for each gene) among different samples independently. The permutated expression read count and methylation intensity of each gene were then used as the input data to *m⁶A-express* and the log-linear to assess the false-positive rate. We observed much fewer genes with small P values close to zero for *m⁶A-express* than the log-linear in all three datasets (Figure 3A), demonstrating a much lower false-positive rate and thus higher specificity for *m⁶A-express*. Particularly, at the significant level of P value = 0.05, *m⁶A-express* committed only ∼1/3 of the false positive predictions by the log-linear (Figure 3B).

We next assessed the prediction precision of the two models. Because the precision could be estimated as $1 - N_p/N_o$, where N_p and $N_o$are the numbers of significant genes in the permuted data (false positives) and the original data (predicted positives), respectively, we applied both models to the original data and prediction P values for each gene (Figure 3C) and then evaluated prediction precisions for 3 data sets (Supplementary Table S6). *m⁶A-express* has higher precisions (0.921–0.967) than the log-linear (0.667–0.852) at the significant level of 0.05, outperforming the log-linear for ∼10–26% (Supplementary Table S6).

Next, we evaluated the prediction sensitivity from the original data by the two models. To control the false discovery rate, we computed FDRs using the BH method. Due to a lack of ground truth of m⁶A-reg-exp genes, we examined the numbers of detected m⁶A-reg-exp genes at FDR < 0.05. Specifically, *m⁶A-express* detected 739 (for M3-KD-HeLa), 491 (for M14-KD-HeLa) and 84 (for M3-KD-HepG2) more significant m⁶A-reg-exp genes than the log-linear (Figure 3D,E). Because *m⁶A-express* has higher precision, this result implies that *m⁶A-express* also had a higher sensitivity than log-linear in all three real datasets (Figure 3D). Taken together, these assessments using the real datasets verified again that *m⁶A-express* could achieve higher specificity and precision while maintaining a greater sensitivity than the log-linear model.

Distinct m⁶A regulation of gene expression in different cancer lines

METTL3 and METTL14 competitively regulate transcription by mediating different m⁶A-reg-exp in Hela cells. To understand the role of human m⁶A methyltransferase METTL3 and METTL14 in mediating m⁶A-reg-exp, we predicted m⁶A-reg-exp in M3-KD-HeLa and M14-KD-HeLa using *m⁶A-express*. Out of 1401 (in M3-KD-HeLa) and 900 (in M14-KD-HeLa) candidate DE-DM genes, *m⁶A-express* identified 813 and 529 significant (FDR < 0.05) m⁶A-reg-exp genes, respectively (Figure 4A). Among them, 710 (87.33%) in M3-KD-HeLa and 475 (89.79%) in M14-KD-HeLa were predicted to have negative β_1 (Figure 4A and Supplementary Figure S8), suggesting that both METTL3 and METTL14 mediated mostly m⁶A-dependent down-regulation of gene expression. Several of these predicted negative regulations are also reported in the m6ADD (73) and m6A2Target (74) databases (Supplementary Table S7). This result supported m⁶A's key role in promoting mRNA decay (34).

We next examined the m⁶A peaks in these m⁶A-reg-exp genes and found an average of ∼1.5 peaks per gene (1054 peaks in 813 genes in M3-KD-HeLa and 835 peaks in 529 genes in M14-KD-HeLa). Meta-gene analysis of peak loci using *Guitar* (51) showed that these peaks were enriched near the stop codon and in the 3'UTR for both cases (Supplementary Figure S9A,B). This enrichment is more pronounced in m⁶A-reg-exp genes than in DE-DM genes (Supplementary Figure S9A,B), echoing the finding that m⁶A sites that regulate mRNA stability are enriched near the stop codon (34). Next, we examined the mRNA turnover of predicted m⁶A-reg-exp genes in M3-KD-HeLa. Because METTL3 KD reduces m⁶A methylation level and YTHDF2 KD depletes binding of YTHDF2, both KDs would lead to increased mRNA lifetime of m⁶A-reg-exp genes. Therefore, we used the mRNA lifetime datasets of METTL3 KD (GSE98856) and YTHDF2 KD (GSE49339) in HeLa cells. Out of 521 hypo-methylated m⁶A-reg-exp genes (DM m⁶A-reg-exp genes with positive peak fold enrichment) after METTL3 KD, 332 (63.7%) showed increased half-life (Figure 4B). In contrast, 98 out of 211 (46.4%) hypo-methylated non-m⁶A-reg-exp genes had increased lifetime after METTL3 KD (Figure 4B). This result demonstrates that the predicted m⁶A-reg-exp genes are significantly enriched with increased lifetime after METTL3 KD (P-value = 1.336×10^{-5}; odds ratio = 2.023; Fisher's exact test). Mechanistically, m⁶A promotes mRNA decay by recruiting the 'reader' proteins including YTH family proteins and among them, YTHDF2 has the strongest affinity to degrade the targeted mRNAs (33,34,75). Therefore, we further examined the enrichment of YTHDF2 binding using the PAR-CLIP-seq dataset that profiled YTHDF2 binding in HeLa cells (GSE49339). Among these 332 genes, 289 (87%) contain YTHDF2-binding clusters that overlap with hypo-m⁶A sites in at least one replicates of the YTHDF2 PAR-CLIP-seq data (Figure 4B and Supplementary Figure S10). We also found that 255 (88.2%) of these 289 m⁶A-reg-exp genes with YTHDF2-binding sites showed increased half-time in the siYTHDF2 lifetime data, consistent with the fact that YTHDF2 is the key reader that the

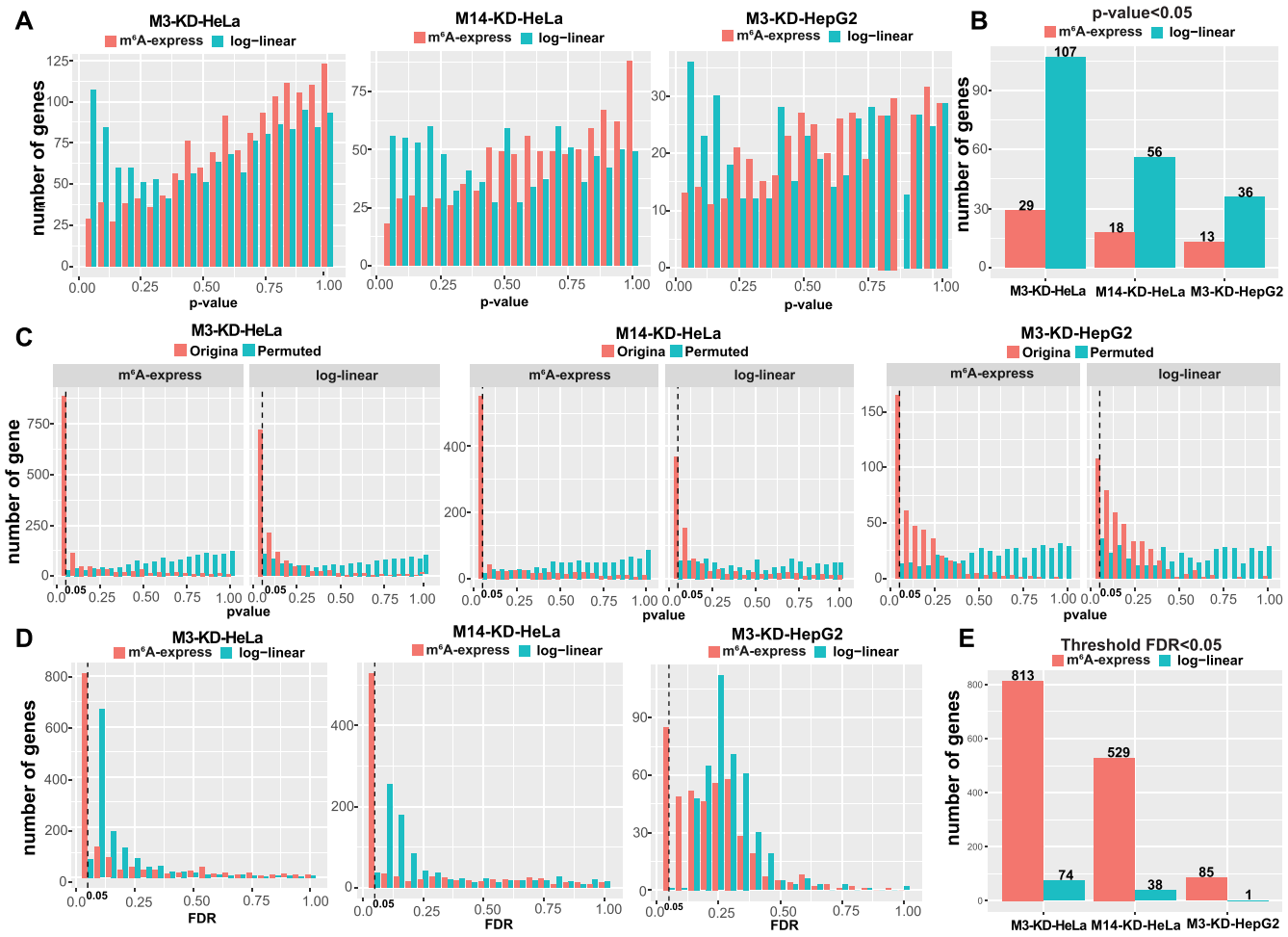

Figure 3. Assessing the specificity, precision, and sensitivity of *m⁶A-express* and log-linear on three real datasets. (**A**) Histograms of the *P* values obtained by *m⁶A-express* (red) and the log-linear (blue) from the three permuted datasets. (**B**) The numbers of false-positive predictions for *P* values < 0.05. (**C**) Each panel shows the histograms of *P* values obtained by *m⁶A-express* and the log-linear from the permuted datasets (blue) and the original datasets (red). (**D**) Histograms of FDRs obtained by *m⁶A-express* (red) and the log-linear (blue), respectively, from the three datasets. The dashed line represents a significant level of FDR = 0.05. (**E**) The numbers of predictions at the significant level of FDR = 0.05.

m^{6}A-dependent decay. In contrast, 68 (69%) out of 98 non-m^{6}A-reg-exp genes with increased lifetime contain hypo-methylated peaks that overlap with YTHDF2 binding sites in at least one YTHDF2 PAR-CLIP-seq replicates (Figure 4B and Supplementary Figure S11). This result shows that these 332 predicted m^{6}A-reg-exp genes with increased life-time are also significantly enriched with YTHDF2 binding than non-m^{6}A-reg-exp genes (*P*-value = 0.0053; odds ratio = 2.054; Fisher's exact test). To further investigate of the difference predicted m^{6}A-reg-exp and non-m^{6}A-reg-exp genes, we checked log2 expression fold-change of the subset of m^{6}A-reg-exp and non-m^{6}A-exp genes with increased life-time and found that lifetime-increased m^{6}A-reg-exp genes are significantly more up-regulated than non-m^{6}A-reg-exp genes after METTL3 KD (*P*-value = 3.696×10^{-9}, *t*-test; Supplementary Figure S12). This result suggests that some predicted non-m^{6}A-exp genes might be regulated by m^{6}A due to increased lifetime, but they are likely associated with less effect on gene expression regulation than predicted m^{6}A-exp genes.

Next, we sought to understand the functions associated with METTL3- or METTL14-mediated m^{6}A-reg-exp in HeLa cells predicted by *m⁶A-express*. We first performed the functional enrichment analysis of m^{6}A-reg-exp genes using the biological process (BP) terms in Gene Ontology (GO). Given that only 86 genes overlap between METTL3- or METTL14-mediated m^{6}A-reg-exp genes (Figure 4C), we expected that METTL3 or METTL14 likely induced highly specific and different functions. To our surprise, both METTL3- and METTL14-mediated m^{6}A-reg-exp genes were enriched mostly in the same set of transcription and RNA processing associated processes (Figure 4D,E). Particularly, transcription by RNA polymerase II was one of the most enriched processes in both cases. METTL3- and METTL14-mediated m^{6}A-reg-exp genes were also enriched in the opposite modes of regulations of transcription-related processes (gene expression, RNA metabolic process, DNA-templated transcription and nucleic acid-templated transcription), with METTL3 associated with the negative and METTL14 with the positive regulations (Fig-

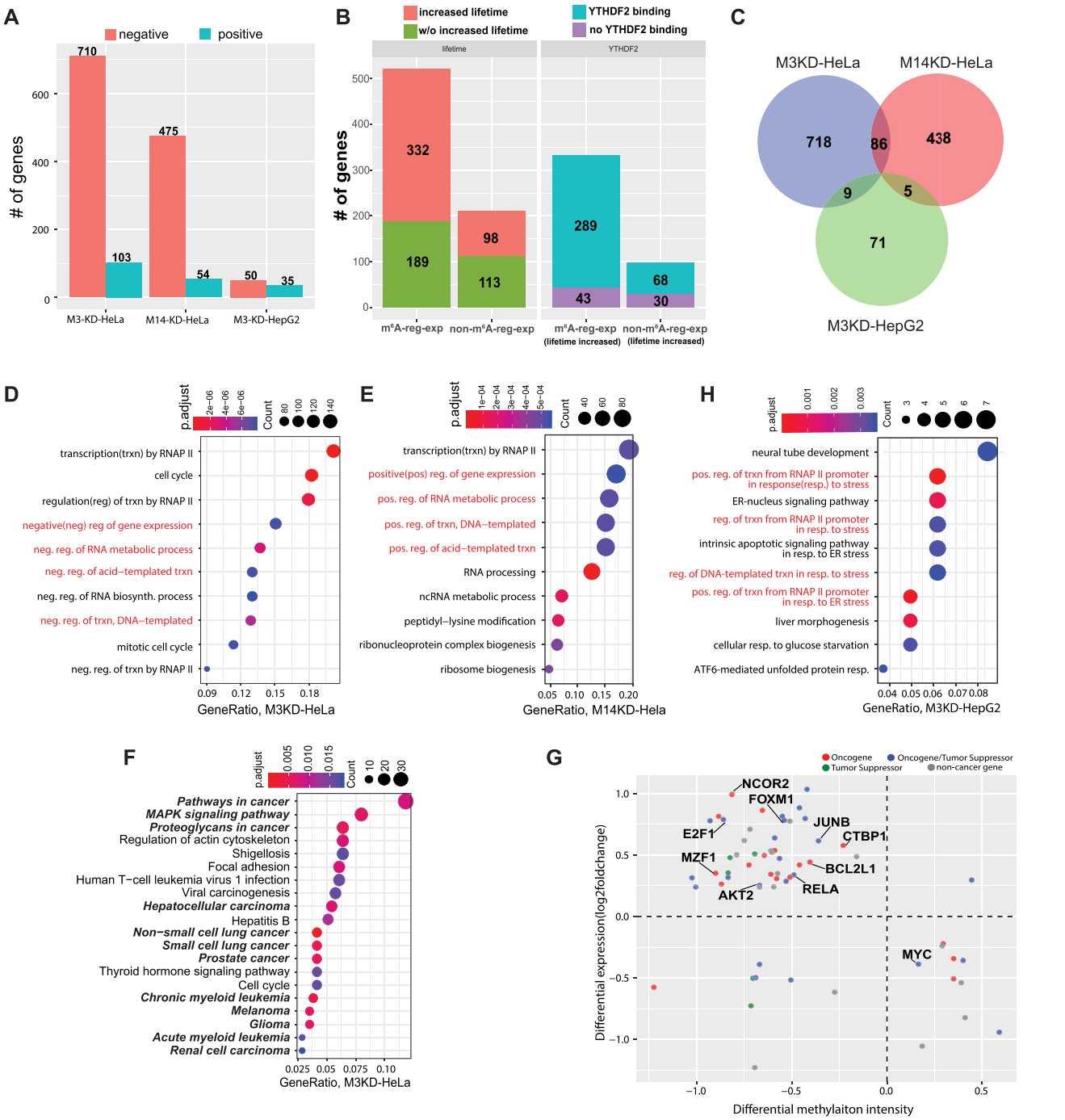

Figure 4. Condition-specific m^{6}A-reg-exp mediated by METTL3 and METTL14 in cancer cell lines. (**A**) The numbers of genes predicted *by m^{6}A-express* to have positive and negative m^{6}A-reg-exp in the three datasets. (**B**) Enrichment of an increased lifetime and YTHDF2 binding in m^{6}A-reg-exp genes. (**C**) Venn diagram showing the overlaps of m^{6}A-reg-exp genes between three datasets. (**D**) Top 10 enriched Gene Ontology Biological Processes in M3-KD-HeLa. (**E**) Top 10 enriched Gene Ontology Biological Processes in M14-KD-HeLa. (**H**) Top 10 enriched Gene Ontology Biological Processes in M3-KD-HepG2. (**F**) Top 20 enriched KEGG pathways in M3-KD-HeLa. (**G**) Scatterplot of differential methylation intensity versus different expression of m^{6}A-reg-exp genes in the top cancer pathways.

ure 4D,E, in red-colored font). Among the genes in these four processes, 112 and 80 of them are METTL3- and METTL14-mediated m^{6}A-reg-exp genes, respectively and between them, only 7 genes are common. We further examined the differential expression of these m^{6}A-reg-exp genes and found that 87 out of 112 and 71 out of 80 of them were up-regulated (Supplementary Table S10). This finding suggests that METTL3 and METTL14 may competitively regulate these transcription-related processes by mediating distinct groups of m^{6}A-reg-exp genes. To further understand the mechanism by which METTL3 and METTL14 may target these transcription-related processes, we examined the enrichment of transcription factors (TFs) in these m^{6}A-reg-exp genes by using TF and TF co-factors in HumanTFDB (76) database. We found a significant enrichment of co-factors in both METTL3-mediated m^{6}A-reg-exp genes (46 out of 112 genes; P-value $= 2.967 \times 10^{-3}$; Fisher's exact test) and METTL14-mediated m^{6}A-reg-exp genes (33 out of 80 genes; P-value $= 1.223 \times 10^{-3}$; Fisher's exact test; Supplementary Figure S13). This result suggests that METTL3 and METTL14 may regulate these transcription-related processes by preferentially targeting m^{6}A-reg-exp of largely different sets of TF co-factors. We further queried the UniProtKB webserver (77) or the molecular function to determine if a transcription factor was a repressor or an activator. We found more repressors among METTL3-associated m^{6}A-reg-exp genes and more activators among METTL14-associated ones (Supplementary Table S11).

Interestingly, 6 out of 7 common m^{6}A-reg-exp genes between the two sets were also TFs including CUX1, ZFHX3, NFIC, FOXM1, RELA and SPEN. Also, the predicted β_1s of three genes (CUX1, ZFHX3 and NFIC) had different signs between M3-KD-HeLa and M14-KD-HeLa, suggested that METTL3 and METTL14 may mediate opposite modes of m^{6}A-dependent regulation of their expressions (positive versus negative regulation) (Supplementary Table S8). Given that their expressions are all up-regulated in METTL3 KD or METTL14 KD versus WT HeLa cells, this result implies that METTL3 and METTL14 may also collaboratively down-regulate the expression of these TFs in HeLa cells by inducing a competitive m^{6}A-dependent regulation of gene expression. Taken together, these results suggested METTL3 and METTL14 may competitively regulate transcription in HeLa cells by mediating m^{6}A-dependent down-regulation of gene expression of different sets of TFs and co-factors.

Besides these competitively regulated transcription-related processes, cell cycle processes were uniquely enriched for METTL3-mediated m^{6}A-reg-exp genes. Several lines of existing research supported the involvement of METTL3 in the regulation of the cell cycle. METTL3 has been shown to inhibit cell cycle progression by regulating m^{6}A-dependent degradation of cyclin D1 (CCND1) mRNA. Consistent with this finding, CCND1 is predicted by *m^{6}A-express* to have a negative regulation (FDR $= 0.021$, $\beta_1 = -0.34$) with up-regulated expression [$\log_2$(Fold-Change) $= 0.28$] after METTL3 KD. In contrast, diverse processes including RNA processing, ncRNA metabolic process, peptidyl-lysine modification, ribonucleoprotein complex biogenesis and ribosome biogenesis, were uniquely enriched in METTL14-mediated m^{6}A-reg-exp genes and the involvement of METTL14 in many of these processes have also been linked in the literature. For instance, TAR RNA-binding protein 2 (TARBP2), an important component of the RNA-induced silencing complex (RISC), was shown to recruit m^{6}A methyltransferase complex to methylate target transcripts and promote their decay (78). Here, we found that METTL14 could also methylate TARBP2 directly to regulate its expression (FDR $=$ 0.0016; $\beta_1 = -0.37$). Also, AGO2 was another METTL14-mediated m^{6}A-reg-exp gene (FDR $= 1.82 \times 10^{-5}$; $\beta_1 = -0.44$). AGO2 is a key protein of RISC that is recruited by microRNAs to silence their target mRNAs. The stability of AGO2 transcripts was shown to be regulated by both METTL3 and METTL14 in an m^{6}A-dependent manner (79). Taken together, these results underscore the complex influences of m^{6}A-reg-exp mediated by METTL3 and METTL14 on the metabolism of transcriptome and other processes (75,80).

We next performed the enrichment of Kyoto Encyclopedia of Genes and Genomes (KEGG) pathways in these m^{6}A-reg-exp genes mediated by METTL3 and METTL14. We found no enriched pathways for METTL14 but significant enrichment for METTL3 in several cancer pathways, a variety of cancers, viruses, and viral carcinoma (Figure 4F). This is consistent with the prevailing evidence that showed proto-/oncogenic role of METTL3 in regulating all these enriched cancer pathways [pathways in cancer, MAPK signaling pathway, proteoglycans in cancer, thyroid hormone signaling pathway and cell cycle (81–83)] and enriched cancers [hepatocellular carcinoma, non-small/small cell lung cancer, prostate cancer, leukemia, melanoma and glioma, and renal cell carcinoma (80,84,85)]. Among the genes in these enriched cancers and cancer pathways, 62 of them are m^{6}A-reg-exp and the participation of 10 genes (FOXM1, NCOR2, E2F1, JUNB, BCL2L1, CTBP1, MZF1, IGF1R, AKT2, RELA, MYC; Figure 4G) in cancers has also been verified in recent studies (86–89). For instance, METTL3 regulates the epithelial-mesenchymal transition through m^{6}A-dependent destabilization of JUNB (90) (FDR $=$ 5.083×10^{-5}, $\beta_1 = -1.025$). A key mechanism of m^{6}A's participation in regulating various cancer is by regulating the gene expressions of cancer-related genes through changing the status of m^{6}A methylations in their mRNAs (89). We consulted TSGene (91) and confirmed that out of 813 METTL3-mediated m^{6}A-reg-exp genes in Hela cell, 67 are tumor suppressors (Supplementary Table S12). Interestingly, 14 of 62 m^{6}A-reg-exp genes in cancer-related pathways are tumor suppressors, yet another evidence of a key mechanism by which METTL3 regulates cancer maybe through mediating m^{6}A-reg-exp of tumor suppressors. We also examined the differential expression versus differential methylation intensity of these 62 m^{6}A-reg-exp genes (Figure 4G) and found that most of them have decreased m^{6}A intensity after METTL13 KD, which is accompanied by up-regulation in gene expression. All of marker genes' expression have been regulated by methylation in a negative form (Figure 4G).

METTL3 induces different m^{6}A regulation of gene expression in HeLa and HepG2 cancer cells. Because METTL3 is found to have highly context-specific roles in regulat-

ing different processes and different types of cancer (92), we sought to understand the context-specific nature of METTL3-mediated m^{6}A-reg-exp. We applied *m^{6}A-express* to the M3-KD-HepG2 MeRIP-seq data and predicted 85 significant (FDR $<$ 0.05) m^{6}A-reg-exp genes. Compared with METTL3-mediated m^{6}A-reg-exp genes in HeLa cells, the number is much smaller and only nine genes are common (Figure 4C). Although a majority of these genes (50 out of 85) were predicted to have negative regulations or negative βs, the percentage (58.82%) is much lower than that (86.27%) in HeLa cells. While the metagene distributions of m^{6}A peaks on the predicted m^{6}A-reg-exp genes showed an enrichment near the stop codon (Supplementary Figure S9C), similar to that from Hela cells, the distinct m^{6}A-reg-exp genes in HeLa and HepG2 cells imply that METTL3-mediated m^{6}A-reg-exp is likely cell-specific.

To understand the relationship between the enriched biological functions of METTL3-mediated m^{6}A-reg-exp in these two cancer cell lines, we performed the over-representation analysis using both BP terms in GO and KEGG pathways. No KEGG pathway was enriched, but highly different biological processes from those for HeLa cells were enriched for HepG2 cells (Figure 4H). Most of these top enriched processes are related to the endoplasmic reticulum (ER) stress-related processes (response to ER stress, intrinsic apoptotic signaling pathway and cellular response to glucose starvation). They are in stark contrast to the enriched transcription and RNA processing-related processes in HeLa cells. Cancer cells are known to cause an accumulation of unfolded proteins, resulting in ER stress, during which transcription and translational reprogramming are tightly regulated (93). The top 2 enriched processes suggested an m^{6}A-dependent regulation of transcription in response to ER stress and some of the involved m^{6}A-reg-exp genes include CEBPB (FDR $= 1.09 \times 10^{-3}$, $\beta_1 = -1.326$), HSPAS (FDR $= 3.27 \times 10^{-5}$, $\beta_1 = 1.012$), ATF4 (FDR $= 7.44 \times 10^{-4}$, $\beta_1 = -1.267$) and XBP1 (FDR $= 5.083 \times 10^{-5}$, $\beta_1 = -0.616$). Regulation of ER stress through m^{6}A-reg-exp has yet been reported and our prediction may point to an undiscovered mechanism of m^{6}A-dependent regulation of ER stress. Overall, this result highlights the context-specific nature of METTL3 mediated m^{6}A-reg-exp.

Organ-specific m^{6}A regulation of gene expression in human tissues

Recent studies have profiled m^{6}A epitranscriptome in adult human tissues and revealed both conserved and tissue-specific m^{6}A methylome (72,94). A key observation reported in (72) is that ubiquitously expressed genes are more likely to be m^{6}A regulated, and among them, the m^{6}A epitranscriptome of brain tissues is highly specific. To extend this finding, we investigated the dynamic m^{6}A methylations within the tissues of different human organs. We hypothesized that these dynamic m^{6}A methylations could regulate gene expression and m^{6}A-reg-exp is organ-specific. To test this hypothesis, we re-analyzed MeRIP-seq samples of adult human tissues (CRA001315, Beijing Institute of Genomics Data Center) and examined the m^{6}A epitranscriptome of brain and intestine tissues, two organs with the largest number of tissue samples, including those from the cerebrum, hypothalamus, cerebellum and brainstem for the brain and the duodenum, jejunum, appendix, rectum and colon for the intestine. Using *exomePeak*, we identified 20 006–21 357 peaks in different brain tissues and 14 690–17 741 peaks in different intestine tissues (Figure 5A). Among them, we identified 10 151 *conserved peaks* in 6248 genes in brain tissues and 7074 conserved m^{6}A peaks in 4797 genes in intestine tissues. This result is consistent with the previous finding that m^{6}A is most abundant in brain tissues. We confirmed that these m^{6}A peaks were enriched near the stop codon and the meta-gene distributions of m^{6}A were similar among all tissue samples (Supplementary Figure S14). We also examined the intensities of these m^{6}A peaks and found that their distributions were similar within brain and intestine tissues but with slightly lower mean intensity in brain tissues (Figure 5B). Next, we focused on conserved m^{6}A peaks that are also highly variable within the brain or intestine tissues. For each conserved peak, we calculated the coefficient of variations (CVs) of their intensities (Materials and Methods section) and selected those with CV $>$ 0.3 as *highly variable peaks* (HVPs). We obtained 3634 and 3503 HVPs in the brain and intestine tissues, respectively, and among them, 609 are shared (Figure 5C). Compared to the conserved stable peaks (CV $<$ 0.3), these HVPs were more organ-specific, with a lower percentage of shared peaks between the brain and intestine (Figure 5C). Consistent with the finding in (72), we also found that intestine tissues' CV values were higher than those in brain tissues (Supplementary Figure S4). Next, we performed the GO enrichment analysis of the genes with these HVPs and found that HVPs in both tissues were most enriched in the same set of general transcription-related pathways (Figure 5D, large gene ratio), along with some tissue-specific pathways (Figure 5D, small gene ratios). This result indicates that even though HVPs are more organ-specific, they are mostly associated with tissue-independent generic transcription pathways.

Then, we applied *m^{6}A-express* to the genes with HVPs and identified 143 m^{6}A-reg-exp genes in brain tissues and 401 m^{6}A-reg-exp genes in intestine tissues. The *Guitar* plots showed that the peaks on these m^{6}A-reg-exp genes centered around the stop codon more than HVPs and the peak distributions in brain and intestine tissues were similar (Supplementary Figure S15). We also found that these m^{6}A-reg-exp genes are markedly organ-specific, with only 13 genes common between the brain and intestine (Figure 5E). Besides, m^{6}A was predicted to down-regulate gene expression (i.e. negative β_1) for all except one m^{6}A-reg-exp gene (Figure 5E), consistent with m^{6}A's key role in promoting mRNA decay. Examining methylation intensities and gene expressions of m^{6}A-reg-exp genes further confirmed this overwhelming negative regulatory relationship (Supplementary Figure S16). Among brain tissues, m^{6}A-reg-exp genes exhibit the highest methylation intensities (and thus lowest expressions) in the hypothalamus but the lowest methylation intensities (and highest expression) in the cerebellum (Supplementary Figure S16A). In contrast, m^{6}A-reg-exp genes showed less variation in both methylation intensity and gene expression in intestine tissues. One exception is the duodenum, where highly divergent methylation and expression levels were observed for m^{6}A-reg-exp genes

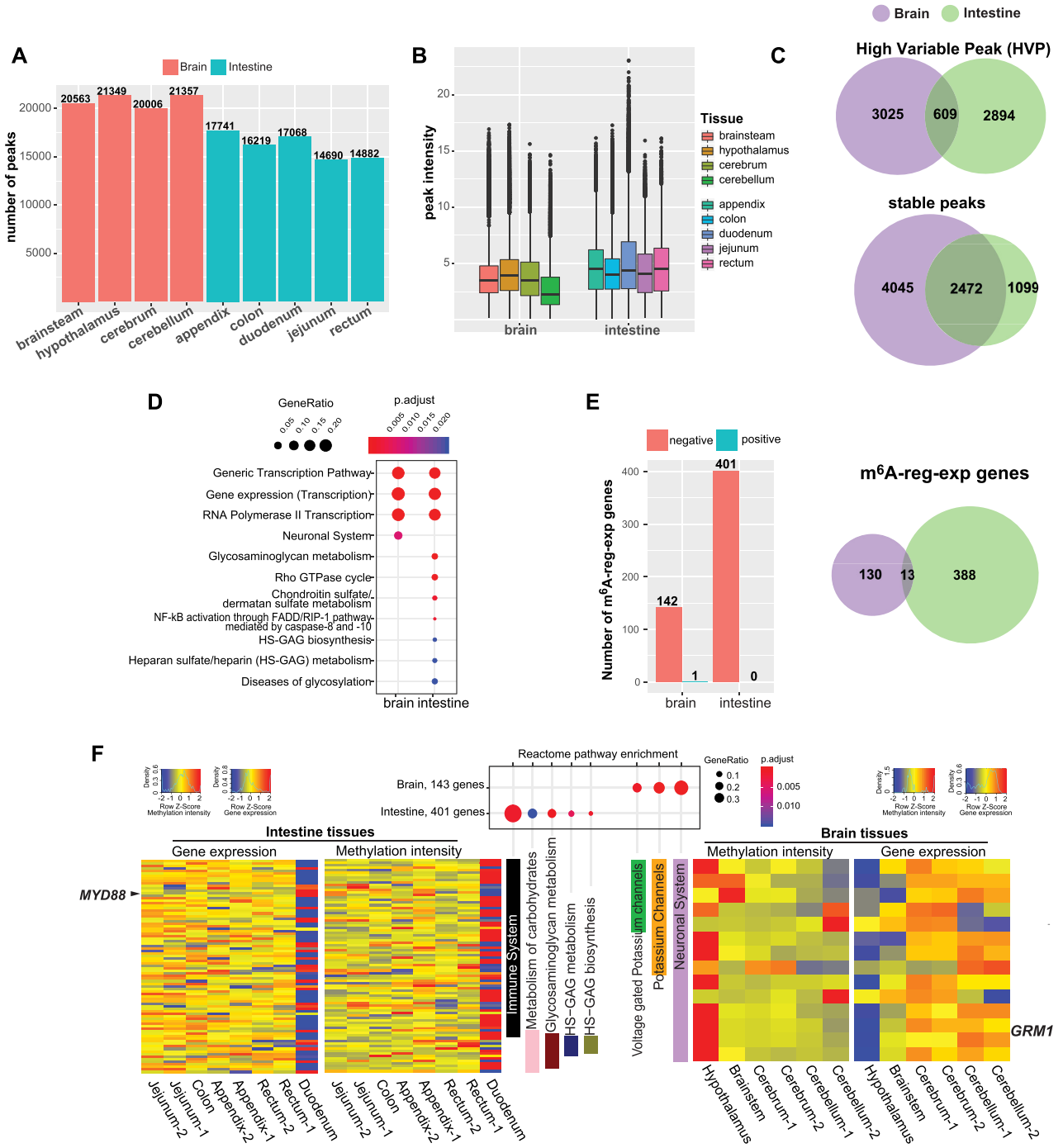

Figure 5. m^{6}A-reg-exp predicted in the brain and intestine. (**A**) The number of peaks in each brain and intestine tissue. (**B**) Boxplot shows the distribution of peak methylation intensity in each brain and intestine tissues. (**C**) Venn diagrams of high variable peaks (HVPs) and stable peaks in the brain and intestine. (**D**) Top enriched Reactome pathways in HVP genes of brain and intestine tissues. (**E**) The number of m^{6}A-reg-exp genes with negative and positive regulation and the Venn diagram of m^{6}A-reg-exp genes in the brain and intestine. (**F**) Top enriched Reactome pathways from 143 and 401 m^{6}A-reg-exp genes of the brain and intestine (middle section). Heatmaps show the methylation intensity and expression of m^{6}A-reg-exp in these enriched processes of the brain (right-hand side panel) and intestine (left-hand side panel).

(Supplementary Figure S16B). Further inspection of the regulatory coefficients β_1 revealed an overall stronger m^{6}A regulation in intestine tissues (Supplementary Figure S17). Next, we conducted the Reactome Pathway enrichment analysis (95) of these m^{6}A-reg-exp genes and found highly organ-specific pathways enriched in the brain and intestine (Figure 5F). For the brain, the neuronal system and the pathways related to neuron ion channels including potassium channels and voltage-gated potassium channels were the most enriched. We found 14 m^{6}A-reg-exp genes in these top enriched pathways for the brain (Figure 5F and Supplementary Table S13). Particularly, m6A-dependent regulation of *GRM1* for cerebellar development has been confirmed (96). The involvement of m^{6}A in regulating brain development and neurophysiological functions including plasticity and learning has been demonstrated (97). Yet, regulating the expression of ion channel-associated genes in an m^{6}A-dependent manner has not been comprehensively studied (96). We found that these 14 genes showed distinct expression patterns in different brain tissues, being barely expressed in the hypothalamus but highly expressed in the cerebrum and cerebellum (Figure 5F, right panel heatmap). We further confirmed these expression patterns using the GTEx database (Supplementary Figure S18). Consistent with the predicted negative regulation by m^{6}A, the m^{6}A methylation intensity is most pronounced in the hypothalamus but significantly decreased in the cerebrum and cerebellum (Figure 5F). Taken together, this result shows that genes involved in the neuronal system exhibit distinct m^{6}A intensity in different brain tissues and the m^{6}A intensity may dynamically control the neuronal system and especially the function of potassium channels in different brain tissues through m^{6}A-dependent down-regulation of gene expressions.

In contrast, the m^{6}A-reg-exp genes in intestine tissues were enriched in the immune system and metabolism-related pathways (Figure 5F). Because the intestine is an important digestive and immune organ for humans, these enriched pathways are consistent with intestine tissues' specific biological functions, further underscoring an organ-specific m^{6}A-regulation of gene expression. A total of 85 m^{6}A-reg-exp genes were identified in the intestine's top pathways (Figure 5F, heatmap of left panel). Like in the brain, diverse m^{6}A intensities and gene expressions are observed for these m^{6}A-reg-exp genes across brain tissues but they clearly present a negative relationship (Figure 5F), confirming the predicted m^{6}A down-regulation of gene expression. Out of these 85 genes, 71 are in the immune system, suggesting that the immune system may be the key process that m^{6}A regulates in the intestine (Figure 5F). Recent studies have recognized m^{6}A as a crucial regulator of the innate and adaptive immune response to bacterial and viral infection (26,98–101). Among the predicted genes (Supplementary Table S13), m6A-dependent regulation of SOCS3's expression in controlling T-cell homeostasis (102) and that of MYD88's expression during inflammatory response in human dental pulp cells (103) have been confirmed. However, m^{6}A's function in the intestine immune system has not been reported. MYD88 functions as an essential innate immune signaling adaptor in the interleukin-1 and Toll-like receptor signaling pathways. MYD88 plays an important role in maintaining intestinal homeostasis and gut-microbiome interactions (104) and exhibits complex, cell-type specific functions (105,106). Indeed, MYD88 showed considerable variation in expression across these intestine tissues and particularly under-expressed in the duodenum. Our result suggests that m^{6}A may regulate the expression of MYD88 to control the immune responses in the intestine.

DISCUSSION

Understanding condition-specific regulatory functions of m^{6}A is a key focus in the current epitranscriptome research. Producing global, unbiased predictions of m^{6}A functions from widely used MeRIP-seq samples could provide testable targets and accelerate the functional discovery. We presented here *m^{6}A-express*, the first algorithm for predicting m^{6}A-regulation of gene expression from limited MeRIP-seq samples collected under specific conditions. *m^{6}A-express* adopts a Bayesian hierarchical model to enable accurate learning of the regulatory relationship between m^{6}A intensity and gene expression from limited samples, a practical constraint in many MeRIP-seq studies.

We extensively assessed the performance of *m^{6}A-express* using both simulated data and real MeRIP-seq samples. Owing to a lack of experimentally validated m^{6}A regulation of gene expression, we simulated this regulation and the resulting data for a treated-versus-control experimental setting using the *m^{6}A-express* model. To closely mimic the data from real experiments, we estimated the distributions of the model parameters and hyper-parameters including the m^{6}A intensity, the regulatory strength, and the number of candidates from the real MeRIP-seq data and used these distributions to guide the simulation. We simulated the data for different replicates, regulatory strengths (weak, medium and strong), and numbers of m^{6}A-reg-exp genes and evaluated *m^{6}A-express*'s performance for estimating the regulatory strength (β_1) and detecting m^{6}A-reg-exp genes. The results showed that *m^{6}A-express* significantly outperformed the log-linear model in all simulated cases and was robust against regulatory strength, the number of m^{6}A-reg-exp genes and especially small sample size. We further validated *m^{6}A-express*'s performance for detecting m^{6}A-reg-exp genes using real MeRIP-seq datasets from three treated-versus-control experiments. Using a gene-permutation strategy, we estimated the prediction false-positive rate of *m^{6}A-express* was only $\sim$1/3 of that of the log-linear model. We also inferred the precision and sensitivity of *m^{6}A-express* in these three datasets and showed $\sim$10–26% and >10-fold improvement in precision and sensitivity, respectively, over the log-linear model. Using the RNA lifetime data, we further demonstrated that the predicted m^{6}A-reg-exp genes in HeLa cells were enriched with genes of an increased lifetime after METTL3 KD. A similar enrichment conclusion holds for YTHDF2 binding in their peaks. Moreover, in all the predictions from these three and the human tissue datasets, we observed an overwhelming m^{6}A down-regulation of gene expression; this outcome is consistent with m^{6}A's main post-transcriptional function to promote mRNA decay.

To demonstrate the utility of *m^{6}A-express*, we examined METTL3- and METTL14-mediated m^{6}A-reg-exp in

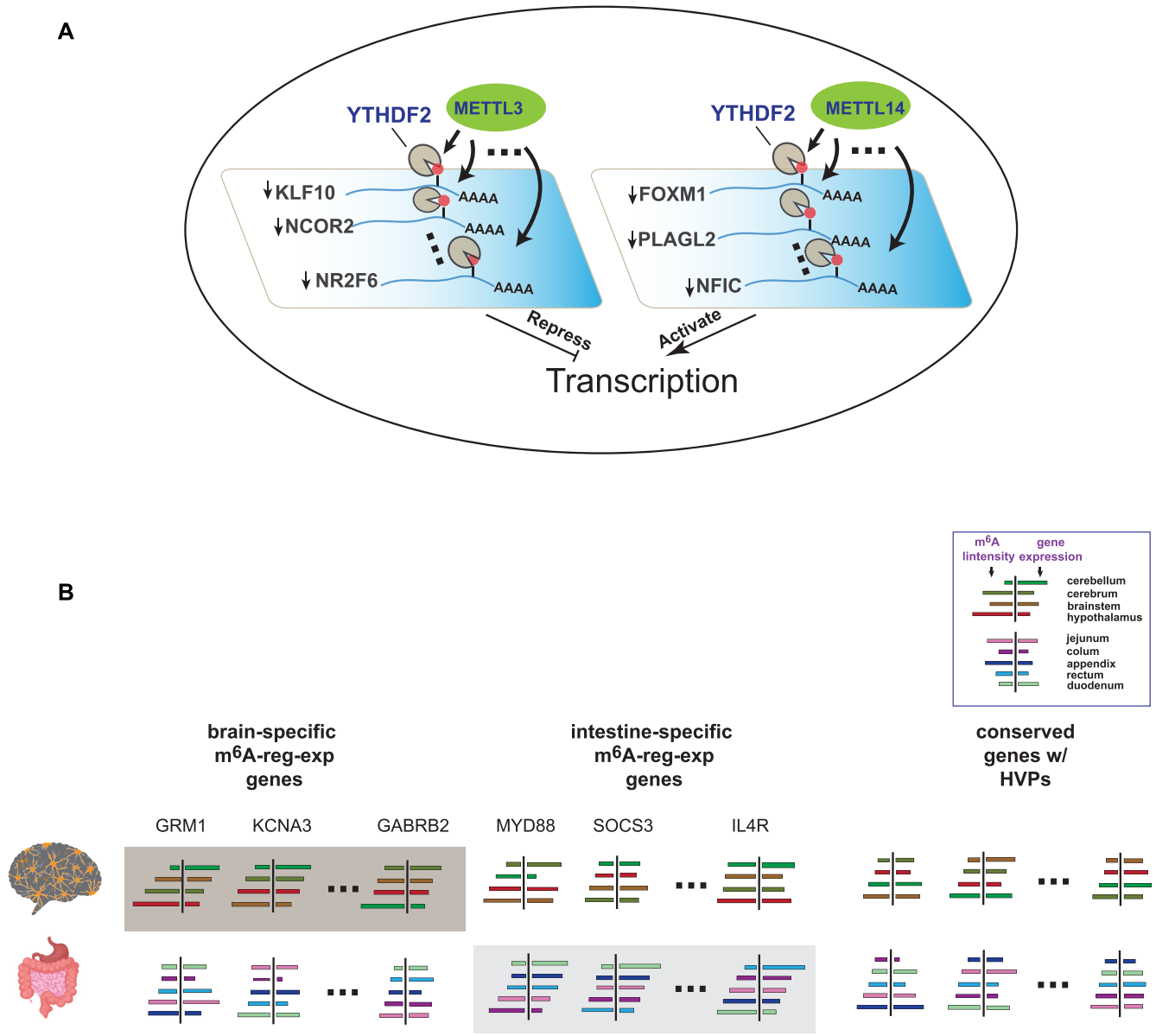

Figure 6. Illustration of uncovered complex and condition-specific m^{6}A regulation of gene expression. (**A**) Competitive regulation of transcription between METTL3- and METTL14-mediated m^{6}A-reg-exp in HeLa cells. METTL3 and METTL14 target different sets of m^{6}A-reg-exp genes involved in processes with opposite regulatory modes of transcription. YTHDF2 is the main reader protein that facilitates this m^{6}A-reg-exp. (**B**) Organ-specific m^{6}A-reg-exp in the brain and intestine (shaded parts), where the dynamic m^{6}A intensities of m^{6}A-reg-exp are predictive of their expression changes.

HeLa cells. We found that METTL3 and METTL14 mediated distinct sets of m^{6}A-reg-exp genes. Intriguingly, these genes were enriched in the opposite modes of regulations of the same transcription-related processes, with METTL3 associated with the negative and METTL14 with the positive regulations. Because the expressions of both sets of m^{6}A-reg-exp were up-regulated in the respective KD cells compared to WT cells, this result suggested a surprising competitive regulation of transcription between METTL3- and METTL14-mediated m^{6}A-reg-exp (Figure 6A). Crystal structural analyses have identified METTL3 as the catalytic component of the METTL3-METTL14 heterodimer but METTL14 as a critical member for recognizing the m^{6}A substrate (107–109). However, depletion of either METTL3 or METTL14 using CRISPR did not show complete removal of m^{6}A but instead generated different m^{6}A profiles in several cell conditions (110–113). A large body of functional studies has also pointed to the distinct roles that METTL3 and METTL14 play in an m^{6}A-dependent manner in controlling normal physiological processes and diseases. METTL14 has also been shown to form a feedback loop with demethylase ALKBH5 to control the m^{6}A methylation (25). These results suggest a complex relationship between METTL3 and METTL14 in modulating m^{6}A's levels and exerting their functional influences. Our finding provides a specific lead to a complex relationship

between METTL3 and METTL14 in regulating transcriptions through their mediated m^{6}A-reg-exp.

m^{6}A is also increasingly recognized as condition-specific, with a subset of sites appearing dynamic in cell types, under physiological conditions, and in response to stimuli (114). Here, by using *m^{6}A-express*, we showed that m^{6}A-reg-exp is also highly cell and tissue type-specific. We first found that METTL13-mediated m^{6}A-reg-exp genes in HeLa and HepG2 cells were highly specific to the cell types and were enriched in distinct biological processes. Then, we uncovered markedly unique m^{6}A-reg-exp in brain and intestine tissues and further revealed that these m^{6}A-reg-exp genes were enriched in the processes important for their respective organ including potassium channels for the brain and immune systems for the intestine. Previous studies highlighted the tissue specificity of m^{6}A peaks in ubiquitously expressed genes (72). Here, we underscore the importance of dynamic relationships between m^{6}A and gene expression. We showed that both m^{6}A intensity and expression levels of m^{6}A-reg-exp genes vary considerably across the tissue samples. Intriguingly, we found that the dynamic changes of m^{6}A intensity alone did not constitute an organ-specific trait, as genes with HVPs are enriched in general, tissue-independent processes. In contrast, only a small subset of HVPs, whose dynamic m^{6}A intensities are predictive of their expression changes by *m^{6}A-express*, are organ-specific and likely to be functional m^{6}A peaks that regulate gene expression (Figure 6B). Moreover, these m^{6}A-reg-exp genes are enriched in unique organ-specific functions that are not shared by those in differentially expressed genes (Supplementary Figure S19), underscoring once again an m^{6}A-dependent, condition-specific regulatory circuitry.

Despite the demonstrated robustness and utility of *m^{6}A-express*, we noticed that a portion of predicted m^{6}A-reg-exp genes after METTL3 KD in HeLa cells are not associated with an increased lifetime. This suggests that the predicted m^{6}A-reg-exp likely includes a mix of targets due to direct and indirect m^{6}A-induced mRNA decay, and it could also capture expression changes due to other modes of m^{6}A regulation of RNAs such as splicing and the co-transcription between m^{6}A and histone modification (115,116). In all the METTL3 KD or METTL14 KD datasets, *m^{6}A-express* also predicted a small set of positively regulated m^{6}A-reg-exp. Although m^{6}A can stabilize mRNA by recruiting the readers IGF2BP1-3, such a mechanism could not be established without additional evidence of binding in these predicted genes by these readers. However, when other data that survey the bindings of different readers and their cofactors are available, *m^{6}A-express* could be extended to include them to separate the targets due to secondary effect and further delineate the specific mode of m^{6}A regulation. This will be a promising future direction for which we plan to improve *m^{6}A-express*.

In conclusion, *m^{6}A-express* is a powerful and efficient new tool that predicts condition-specific m^{6}A regulation of gene expression in the m^{6}A methylome (running speed shown in Supplementary Table S9). We demonstrated its utility with real samples from experiments with a general setup, which can survey global m^{6}A-reg-exp for the treated-versus-control experiments or interrogate the dynamic regulatory profiles across multiple experimental conditions or tissue samples. Given the intense current interest in condition-specific m^{6}A functions, we believe that *m^{6}A-express* is a timely tool that will advance our understanding of m^{6}A's regulatory mechanisms in particular and the m^{6}A research in general.

DATA AVAILABILITY

m^{6}A-express is implemented as a python/R package and is freely available at https://github.com/Yufei-Huang-Lab/m6Aexpress. This package is based on the software $R \geq 3.5$ and python 3. The source code and the instruction of the *m^{6}A-express* package can be found at the website. The sources of all real MeRIP-seq data are described in Materials and Methods section.

SUPPLEMENTARY DATA

Supplementary Data are available at NAR Online.

ACKNOWLEDGEMENTS

Authors' contributions: T.Z., S.W.Z., Y.C. and Y.H. conceived the study. T.Z. collected the data, developed the *m^{6}A-express* model and built the package. T.Z. and S.Y.Z. conducted experiments and analyzed the data. T.Z., Y.H., Y.C., S.W.Z., S.J.G. and S.Y.Z. interpreted the results. T.Z., Y.C. and Y.H. wrote the manuscript and all authors revised it. All authors read and approved the final manuscript.

FUNDING

National Natural Science Foundation of China [61873202, 61473232 to S.W.Z.]; China Postdoctoral Science Foundation [2020M683568 to S.Y.Z.]. Funding for open access charge: National Natural Science Foundation of China [61873202, 61473232 to S.W.Z.]; China Postdoctoral Science Foundation [2020M683568 to S.Y.Z.].
Conflict of interest statement. None declared.

REFERENCES

1. Ping,X.L., Sun,B.F., Wang,L., Xiao,W., Yang,X., Wang,W.J., Adhikari,S., Shi,Y., Lv,Y., Chen,Y.S. *et al.* (2014) Mammalian WTAP is a regulatory subunit of the RNA N6-methyladenosine methyltransferase. *Cell Res.* **24**, 177–189.
2. Wang,Y., Li,Y., Toth,J.I., Petroski,M.D., Zhang,Z. and Zhao,J.C. (2014) N6-methyladenosine modification destabilizes developmental regulators in embryonic stem cells. *Nat. Cell Biol.*, **16**, 191–198.
3. Xiao,W., Adhikari,S., Dahal,U., Chen,Y.-S., Hao,Y.-J., Sun,B.-F., Sun,H.-Y., Li,A., Ping,X.-L. and Lai,W.-Y. (2016) Nuclear m 6 A Reader YTHDC1 Regulates mRNA Splicing. *Mol. Cell*, **61**, 507–519.
4. Wang,X., Zhao,B.S., Roundtree,I.A., Lu,Z., Han,D., Ma,H., Weng,X., Chen,K., Shi,H. and He,C. (2015) N(6)-methyladenosine Modulates Messenger RNA Translation Efficiency. *Cell*, **161**, 1388–1399.
5. Zhou,J., Wan,J., Gao,X., Zhang,X., Jaffrey,S.R. and Qian,S.B. (2015) Dynamic m(6)A mRNA methylation directs translational control of heat shock response. *Nature*, **526**, 591–594.
6. Fustin,J.-M., Doi,M., Yamaguchi,Y., Hida,H., Nishimura,S., Yoshida,M., Isagawa,T., Morioka,Masaki S., Kakeya,H., Manabe,I *et al.* (2013) RNA-methylation-dependent RNA processing controls the speed of the circadian clock. *Cell*, **155**, 793–806.

7. Zheng,G., Dahl,J.A., Niu,Y., Fedorcsak,P., Huang,C.M., Li,C.J., Vagbo,C.B., Shi,Y., Wang,W.L., Song,S.H. *et al.* (2013) ALKBH5 is a mammalian RNA demethylase that impacts RNA metabolism and mouse fertility. *Mol. Cell*, **49**, 18–29.
8. Slobodin,B., Han,R., Calderone,V., Vrielink,J.A., Loayza-Puch,F., Elkon,R. and Agami,R. (2017) Transcription impacts the efficiency of mRNA translation via co-transcriptional N6-adenosine methylation. *Cell*, **169**, 326–337.
9. Meyer,K.D., Saletore,Y., Zumbo,P., Elemento,O., Mason,C.E. and Jaffrey,S.R. (2012) Comprehensive analysis of mRNA methylation reveals enrichment in 3' UTRs and near stop codons. *Cell*, **149**, 1635–1646.
10. Jia,G., Fu,Y., Zhao,X., Dai,Q., Zheng,G., Yang,Y., Yi,C., Lindahl,T., Pan,T. and Yang,Y.-G. (2011) N6-methyladenosine in nuclear RNA is a major substrate of the obesity-associated FTO. *Nat. Chem. Biol.*, **7**, 885–887.
11. Nilsen,T.W. (2014) Internal mRNA methylation finally finds functions. *Science*, **343**, 1207–1208.
12. Zheng,G., Dahl,J.A., Niu,Y., Fedorcsak,P., Huang,C.M., Li,C.J., Vågbø,C.B., Shi,Y., Wang,W.L., Song,S.H. *et al.* (2013) ALKBH5 is a mammalian RNA demethylase that impacts RNA metabolism and mouse fertility. *Mol. Cell*, **49**, 18–29.
13. Hess,M.E., Hess,S., Meyer,K.D., Verhagen,L.A., Koch,L., Bronneke,H.S., Dietrich,M.O., Jordan,S.D., Saletore,Y., Elemento,O. *et al.* (2013) The fat mass and obesity associated gene (Fto) regulates activity of the dopaminergic midbrain circuitry. *Nat. Neurosci.*, **16**, 1042–1048.
14. Chelmicki,T., Roger,E., Teissandier,A., Rucli,S., Dossin,F., Dura,M., Fouassier,C., Lameiras,S. and Bourc'his,D. (2021) m6A RNA methylation regulates the fate of endogenous retroviruses. *Nature*, **591**, 312–316.
15. Lence,T., Akhtar,J., Bayer,M., Schmid,K., Spindler,L., Ho,C.H., Kreim,N., Andrade-Navarro,M.A., Poeck,B., Helm,M. *et al.* (2016) m6A modulates neuronal functions and sex determination in Drosophila. *Nature*, **540**, 242–247.
16. Haussmann,I.U., Bodi,Z., Sanchez-Moran,E., Mongan,N.P., Archer,N., Fray,R.G. and Soller,M. (2016) m6A potentiates Sxl alternative pre-mRNA splicing for robust Drosophila sex determination. *Nature*, **540**, 301–304.
17. Geula,S., Moshitch-Moshkovitz,S., Dominissini,D., Mansour,A.A., Kol,N., Salmon-Divon,M., Hershkovitz,V., Peer,E., Mor,N., Manor,Y.S. *et al.* (2015) Stem cells. m6A mRNA methylation facilitates resolution of naive pluripotency toward differentiation. *Science*, **347**, 1002–1006.
18. Batista,P.J., Molinie,B., Wang,J., Qu,K., Zhang,J., Li,L., Bouley,D.M., Lujan,E., Haddad,B., Daneshvar,K. *et al.* (2014) m(6)A RNA modification controls cell fate transition in mammalian embryonic stem cells. *Cell Stem Cell*, **15**, 707–719.
19. Chen,T., Hao,Y.J., Zhang,Y., Li,M.M., Wang,M., Han,W., Wu,Y., Lv,Y., Hao,J., Wang,L. *et al.* (2015) m(6)A RNA methylation is regulated by microRNAs and promotes reprogramming to pluripotency. *Cell Stem Cell*, **16**, 289–301.
20. Schwartz,S., Mumbach,M.R., Jovanovic,M., Wang,T., Maciag,K., Bushkin,G.G., Mertins,P., Ter-Ovanesyan,D., Habib,N., Cacchiarelli,D. *et al.* (2014) Perturbation of m6A writers reveals two distinct classes of mRNA methylation at internal and 5' sites. *Cell Rep.*, **8**, 284–296.
21. Li,Z., Weng,H., Su,R., Weng,X., Zuo,Z., Li,C., Huang,H., Nachtergaele,S., Dong,L., Hu,C. *et al.* (2017) FTO Plays an Oncogenic Role in Acute Myeloid Leukemia as a N6-Methyladenosine RNA Demethylase. *Cancer Cell*, **31**, 127–141.
22. Zhang,C., Samanta,D., Lu,H., Bullen,J.W., Zhang,H., Chen,I., He,X. and Semenza,G.L. (2016) Hypoxia induces the breast cancer stem cell phenotype by HIF-dependent and ALKBH5-mediated m6A-demethylation of NANOG mRNA. *Proc. Natl. Acad. Sci. U.S.A.*, **113**, E2047–E2056.
23. Keith,B. and Simon,M.C. (2007) Hypoxia-inducible factors, stem cells, and cancer. *Cell*, **129**, 465–472.
24. Lin,S., Choe,J., Du,P., Triboulet,R. and Gregory,R.I. (2016) The mA methyltransferase METTL3 promotes translation in human cancer cells. *Mol. Cell*, **62**, 335–345.
25. Panneerdoss,S., Eedunuri,V.K., Yadav,P., Timilsina,S., Rajamanickam,S., Viswanadhapalli,S., Abdelfattah,N., Onyeagucha,B.C., Cui,X., Lai,Z. *et al.* (2018) Cross-talk among writers, readers, and erasers of m(6)A regulates cancer growth and progression. *Sci. Adv.*, **4**, eaar8263.
26. Lichinchi,G., Gao,S., Saletore,Y., Gonzalez,G.M., Bansal,V., Wang,Y., Mason,C.E. and Rana,T.M. (2016) Dynamics of the human and viral m(6)A RNA methylomes during HIV-1 infection of T cells. *Nat Microbiol*, **1**, 16011.
27. Kennedy,E.M., Bogerd,H.P., Kornepati,A.V., Kang,D., Ghoshal,D., Marshall,J.B., Poling,B.C., Tsai,K., Gokhale,N.S., Horner,S.M. *et al.* (2016) Posttranscriptional m(6)A editing of HIV-1 mRNAs enhances viral gene expression. *Cell Host Microbe*, **19**, 675–685.
28. Fleming,A.M., Nguyen,N.L. and Burrows,C.J. (2019) Colocalization of m6A and G-quadruplex-forming sequences in viral RNA (HIV, Zika, Hepatitis B, and SV40) suggests topological control of adenosine N 6-methylation. *ACS Central Sci.*, **5**, 218–228.
29. Lichinchi,G., Zhao,B.S., Wu,Y., Lu,Z., Qin,Y., He,C. and Rana,T.M. (2016) Dynamics of human and viral RNA methylation during Zika virus infection. *Cell Host Microbe*, **20**, 666–673.
30. Tan,B., Liu,H., Zhang,S., da Silva,S.R., Zhang,L., Meng,J., Cui,X., Yuan,H., Sorel,O., Zhang,S.W. *et al.* (2018) Viral and cellular N(6)-methyladenosine and N(6),2'-O-dimethyladenosine epitranscriptomes in the KSHV life cycle. *Nat. Microbiol.*, **3**, 108–120.
31. Xiao,S., Cao,S., Huang,Q., Xia,L., Deng,M., Yang,M., Jia,G., Liu,X., Shi,J. and Wang,W. (2019) The RNA N 6-methyladenosine modification landscape of human fetal tissues. *Nat. Cell Biol.*, **21**, 651–661.
32. Shi,H., Wei,J. and He,C. (2019) Where, when, and how: context-dependent functions of rna methylation writers, readers, and erasers. *Mol. Cell*, **74**, 640–650.
33. Du,H., Zhao,Y., He,J., Zhang,Y., Xi,H., Liu,M., Ma,J. and Wu,L. (2016) YTHDF2 destabilizes m 6 A-containing RNA through direct recruitment of the CCR4–NOT deadenylase complex. *Nat. Commun.*, **7**, 12626.
34. Wang,X., Lu,Z., Gomez,A., Hon,G.C., Yue,Y., Han,D., Fu,Y., Parisien,M., Dai,Q., Jia,G. *et al.* (2014) N6-methyladenosine-dependent regulation of messenger RNA stability. *Nature*, **505**, 117–120.
35. Huang,H., Weng,H., Sun,W., Qin,X., Shi,H., Wu,H., Zhao,B.S., Mesquita,A., Liu,C. and Yuan,C.L. (2018) Recognition of RNA N 6-methyladenosine by IGF2BP proteins enhances mRNA stability and translation. *Nat. Cell Biol.*, **20**, 285.
36. Dominissini,D., Moshitch-Moshkovitz,S., Schwartz,S., Salmon-Divon,M., Ungar,L., Osenberg,S., Cesarkas,K., Jacob-Hirsch,J., Amariglio,N., Kupiec,M. *et al.* (2012) Topology of the human and mouse m6A RNA methylomes revealed by m6A-seq. *Nature*, **485**, 201–206.
37. Liu,Z., Xiao,X., Yu,D.-J., Jia,J., Qiu,W.-R. and Chou,K.-C. (2016) pRNAm-PC: Predicting N 6-methyladenosine sites in RNA sequences via physical–chemical properties. *Anal. Biochem.*, **497**, 60–67.
38. Chen,W., Feng,P., Ding,H., Lin,H. and Chou,K.-C. (2015) iRNA-Methyl: Identifying N 6-methyladenosine sites using pseudo nucleotide composition. *Anal. Biochem.*, **490**, 26–33.
39. Zhou,Y., Zeng,P., Li,Y.-H., Zhang,Z. and Cui,Q. (2016) SRAMP: prediction of mammalian N6-methyladenosine (m6A) sites based on sequence-derived features. *Nucleic Acids Res.*, **44**, e91.
40. Xiang,S., Liu,K., Yan,Z., Zhang,Y. and Sun,Z. (2016) RNAMethPre: a web server for the prediction and query of mRNA m 6 A sites. *PLoS One*, **11**, e0162707.
41. Xing,P., Su,R., Guo,F. and Wei,L. (2017) Identifying N6-methyladenosine sites using multi-interval nucleotide pair position specificity and support vector machine. *Sci. Rep.*, **7**, 46757.
42. Chen,W., Tang,H. and Lin,H. (2017) MethyRNA: a web server for identification of N6-methyladenosine sites. *J. Biomol. Struct. Dyn.*, **35**, 683–687.
43. Chen,K., Wei,Z., Zhang,Q., Wu,X., Rong,R., Lu,Z., Su,J., de Magalhaes,J.P., Rigden,D.J. and Meng,J. (2019) WHISTLE: a high-accuracy map of the human N6-methyladenosine (m6A) epitranscriptome predicted using a machine learning approach. *Nucleic Acids Res.*, **47**, e41.
44. Meng,J., Cui,X., Rao,M.K., Chen,Y. and Huang,Y. (2013) Exome-based analysis for RNA epigenome sequencing data. *Bioinformatics*, **29**, 1565–1567.

45. Meng,J., Lu,Z., Liu,H., Zhang,L., Zhang,S., Chen,Y., Rao,M.K. and Huang,Y. (2014) A protocol for RNA methylation differential analysis with MeRIP-Seq data and exomePeak R/Bioconductor package. *Methods*, **69**, 274–281.
46. Cui,X., Meng,J., Zhang,S., Chen,Y. and Huang,Y. (2016) A novel algorithm for calling mRNA m6A peaks by modeling biological variances in MeRIP-seq data. *Bioinformatics*, **32**, i378–i385.
47. Zhang,S.-Y., Zhang,S.-W., Fan,X.-N., Meng,J., Chen,Y., Gao,S.-J. and Huang,Y. (2019) Global analysis of N6-methyladenosine functions and its disease association using deep learning and network-based methods. *PLoS Comput. Biol.*, **15**, e1006663.
48. Cui,X., Zhang,L., Meng,J., Rao,M., Chen,Y. and Huang,Y. (2015) MeTDiff: a novel differential RNA methylation analysis for MeRIP-Seq data. *IEEE/ACM Trans. Comput. Biol. Bioinform.*, **15**, 526–534.
49. Liu,L., Zhang,S.W., Huang,Y. and Meng,J. (2017) QNB: differential RNA methylation analysis for count-based small-sample sequencing data with a quad-negative binomial model. *BMC Bioinformatics*, **18**, 387.
50. Zhang,Z., Zhan,Q., Eckert,M., Zhu,A., Chryplewicz,A., De Jesus,D.F., Ren,D., Kulkarni,R.N., Lengyel,E., He,C. *et al.* (2019) RADAR: differential analysis of MeRIP-seq data with a random effect model. *Genome Biol.*, **20**, 294.
51. Cui,X., Wei,Z., Zhang,L., Liu,H., Sun,L., Zhang,S.-W., Huang,Y. and Meng,J. (2016) Guitar: an R/Bioconductor package for gene annotation guided transcriptomic analysis of RNA-related genomic features. *Biomed. Res. Int.*, **2016**, 8367534.
52. Su,R., Dong,L., Li,C., Nachtergaele,S., Wunderlich,M., Qing,Y., Deng,X., Wang,Y., Weng,X. and Hu,C. (2018) R-2HG exhibits anti-tumor activity by targeting FTO/m6A/MYC/CEBPA signaling. *Cell*, **172**, 90–105.
53. Weng,H., Huang,H., Wu,H., Qin,X., Zhao,B.S., Dong,L., Shi,H., Skibbe,J., Shen,C. and Hu,C. (2018) METTL14 inhibits hematopoietic stem/progenitor differentiation and promotes leukemogenesis via mRNA m6A modification. *Cell Stem Cell*, **22**, 191–205.
54. Shen,C., Sheng,Y., Zhu,A.C., Robinson,S., Jiang,X., Dong,L., Chen,H., Su,R., Yin,Z. and Li,W. (2020) RNA demethylase ALKBH5 selectively promotes tumorigenesis and cancer stem cell self-renewal in acute myeloid leukemia. *Cell Stem Cell*, **27**, 64–80.
55. Wang,J., Li,Y., Wang,P., Han,G., Zhang,T., Chang,J., Yin,R., Shan,Y., Wen,J. and Xie,X. (2020) Leukemogenic Chromatin Alterations Promote AML Leukemia Stem Cells via a KDM4C-ALKBH5-AXL Signaling Axis. *Cell Stem Cell*, **27**, 81–97.
56. Bertero,A., Brown,S., Madrigal,P., Osnato,A., Ortmann,D., Yiangou,L., Kadiwala,J., Hubner,N.C., de Los Mozos,I.R. and Sadée,C. (2018) The SMAD2/3 interactome reveals that TGFβ controls m 6 A mRNA methylation in pluripotency. *Nature*, **555**, 256–259.
57. Liu,J., Eckert,M.A., Harada,B.T., Liu,S.-M., Lu,Z., Yu,K., Tienda,S.M., Chryplewicz,A., Zhu,A.C. and Yang,Y. (2018) m 6 A mRNA methylation regulates AKT activity to promote the proliferation and tumorigenicity of endometrial cancer. *Nat. Cell Biol.*, **20**, 1074–1083.
58. Merkurjev,D., Hong,W.-T., Iida,K., Oomoto,I., Goldie,B.J., Yamaguti,H., Ohara,T., Kawaguchi,S.-y., Hirano,T. and Martin,K.C. (2018) Synaptic N 6-methyladenosine (m 6 A) epitranscriptome reveals functional partitioning of localized transcripts. *Nat. Neurosci.*, **21**, 1004–1014.
59. Zhang,S.Y., Zhang,S.W., Liu,L., Meng,J. and Huang,Y. (2016) m6A-Driver: identifying context-specific mRNA m6A methylation-driven gene interaction networks. *PLoS Comput. Biol.*, **12**, e1005287.
60. Zhang,S.-Y., Zhang,S.-W., Fan,X.-N., Zhang,T., Meng,J. and Huang,Y. (2019) FunDMDeep-m6A: identification and prioritization of functional differential m6A methylation genes. *Bioinformatics*, **35**, i90–i98.
61. Tang,Y., Chen,K., Wu,X., Wei,Z., Song,B., Zhang,S., Huang,Y. and Meng,J. (2019) DRUM: Inference of disease-associated m6A RNA methylation sites from a multi-layer heterogeneous network. *Front. Genet.*, **10**, 266.
62. An,S., Huang,W., Huang,X., Cun,Y., Cheng,W., Sun,X., Ren,Z., Chen,Y., Chen,W. and Wang,J. (2020) Integrative network analysis identifies cell-specific trans regulators of m6A. *Nucleic Acids Res.*, **48**, 1715–1729.
63. Garcia-Campos,M.A., Edelheit,S., Toth,U., Safra,M., Shachar,R., Viukov,S., Winkler,R., Nir,R., Lasman,L., Brandis,A. *et al.* (2019) Deciphering the "m(6)A Code" via Antibody-Independent Quantitative Profiling. *Cell*, **178**, 731–747.
64. Liu,H., Begik,O., Lucas,M.C., Ramirez,J.M., Mason,C.E., Wiener,D., Schwartz,S., Mattick,J.S., Smith,M.A. and Novoa,E.M. (2019) Accurate detection of m(6)A RNA modifications in native RNA sequences. *Nat. Commun.*, **10**, 4079.
65. Anders,S. and Huber,W. (2010) Differential expression analysis for sequence count data. *Genome Biol.*, **11**, R106.
66. Liao,Y., Smyth,G.K. and Shi,W. (2019) The R package Rsubread is easier, faster, cheaper and better for alignment and quantification of RNA sequencing reads. *Nucleic Acids Res.*, **47**, e47.
67. Love,M.I., Huber,W. and Anders,S. (2014) Moderated estimation of fold change and dispersion for RNA-seq data with DESeq2. *Genome Biol.*, **15**, 550.
68. Zhang,S., Zhao,B.S., Zhou,A., Lin,K., Zheng,S., Lu,Z., Chen,Y., Sulman,E.P., Xie,K., Bogler,O. *et al.* (2017) m(6)A demethylase ALKBH5 maintains tumorigenicity of glioblastoma stem-like cells by sustaining FOXM1 expression and cell proliferation program. *Cancer Cell*, **31**, 591–606.
69. Edupuganti,R.R., Geiger,S., Lindeboom,R.G.H., Shi,H., Hsu,P.J., Lu,Z., Wang,S.Y., Baltissen,M.P.A., Jansen,P., Rossa,M. *et al.* (2017) N(6)-methyladenosine (m(6)A) recruits and repels proteins to regulate mRNA homeostasis. *Nat. Struct. Mol. Biol.*, **24**, 870–878.
70. Benjamini,Y., Drai,D., Elmer,G., Kafkafi,N. and Golani,I. (2001) Controlling the false discovery rate in behavior genetics research. *Behav. Brain Res.*, **125**, 279–284.
71. Corcoran,D.L., Georgiev,S., Mukherjee,N., Gottwein,E., Skalsky,R.L., Keene,J.D. and Ohler,U. (2011) PARalyzer: definition of RNA binding sites from PAR-CLIP short-read sequence data. *Genome Biol.*, **12**, R79.
72. Liu,J., Li,K., Cai,J., Zhang,M., Zhang,X., Xiong,X., Meng,H., Xu,X., Huang,Z., Peng,J. *et al.* (2020) Landscape and Regulation of m(6)A and m(6)Am Methylome across Human and Mouse Tissues. *Mol. Cell*, **77**, 426–440.
73. Zhou,D., Wang,H., Bi,F., Xing,J., Gu,Y., Wang,C., Zhang,M., Huang,Y., Zeng,J., Wu,Q. *et al.* (2021) M6ADD: a comprehensive database of m(6)A modifications in diseases. *RNA Biol.*, https://doi.org/10.1080/15476286.2021.1913302.
74. Deng,S., Zhang,H., Zhu,K., Li,X., Ye,Y., Li,R., Liu,X., Lin,D., Zuo,Z. and Zheng,J. (2021) M6A2Target: a comprehensive database for targets of m6A writers, erasers and readers. *Brief. Bioinform.*, **22**, bbaa055.
75. Zhao,B.S., Roundtree,I.A. and He,C. (2017) Post-transcriptional gene regulation by mRNA modifications. *Nat. Rev. Mol. Cell Biol.*, **18**, 31–42.
76. Hu,H., Miao,Y.R., Jia,L.H., Yu,Q.Y., Zhang,Q. and Guo,A.Y. (2019) AnimalTFDB 3.0: a comprehensive resource for annotation and prediction of animal transcription factors. *Nucleic Acids Res.*, **47**, D33–D38.
77. UniProt,C. (2021) UniProt: the universal protein knowledgebase in 2021. *Nucleic Acids Res.*, **49**, D480–D489.
78. Fish,L., Navickas,A., Culbertson,B., Xu,Y., Nguyen,H.C.B., Zhang,S., Hochman,M., Okimoto,R., Dill,B.D., Molina,H. *et al.* (2019) Nuclear TARBP2 drives oncogenic dysregulation of RNA splicing and decay. *Mol. Cell*, **75**, 967–981.
79. Min,K.W., Zealy,R.W., Davila,S., Fomin,M., Cummings,J.C., Makowsky,D., McDowell,C.H., Thigpen,H., Hafner,M., Kwon,S.H. *et al.* (2018) Profiling of m6A RNA modifications identified an age-associated regulation of AGO2 mRNA stability. *Aging Cell*, **17**, e12753.
80. Fitzsimmons,C.M. and Batista,P.J. (2019) It's complicated… m(6)A-dependent regulation of gene expression in cancer. *Biochim. Biophys. Acta Gene Regul. Mech.*, **1862**, 382–393.
81. Wu,C.H., Yeh,C.T. and Lin,K.H. (2020) Thyroid hormones suppress FOXM1 expression to reduce liver cancer progression. *Oncol. Rep.*, **44**, 1686–1698.
82. Du,J., Hou,K., Mi,S., Ji,H., Ma,S., Ba,Y., Hu,S., Xie,R. and Chen,L. (2020) Malignant evaluation and clinical prognostic values of m6A RNA methylation regulators in glioblastoma. *Front. Oncol.*, **10**, 208.

83. Yang,Z., Wang,T., Wu,D., Min,Z., Tan,J. and Yu,B. (2020) RNA N6-methyladenosine reader IGF2BP3 regulates cell cycle and angiogenesis in colon cancer. *J. Exp. Clin. Cancer Res.*, **39**, 203.
84. Chen,X.Y., Zhang,J. and Zhu,J.S. (2019) The role of m(6)A RNA methylation in human cancer. *Mol. Cancer*, **18**, 103.
85. He,L., Li,H., Wu,A., Peng,Y., Shu,G. and Yin,G. (2019) Functions of N6-methyladenosine and its role in cancer. *Mol. Cancer*, **18**, 176.
86. De Jesus,D.F., Zhang,Z., Kahraman,S., Brown,N.K., Chen,M., Hu,J., Gupta,M.K., He,C. and Kulkarni,R.N. (2019) m(6)A mRNA methylation regulates human beta-cell biology in physiological states and in type 2 diabetes. *Nat Metab*, **1**, 765–774.
87. Liu,J., Eckert,M.A., Harada,B.T., Liu,S.M., Lu,Z., Yu,K., Tienda,S.M., Chryplewicz,A., Zhu,A.C., Yang,Y. *et al.* (2018) m(6)A mRNA methylation regulates AKT activity to promote the proliferation and tumorigenicity of endometrial cancer. *Nat. Cell Biol.*, **20**, 1074–1083.
88. Sui,B.D., Zheng,C.X., Li,M., Jin,Y. and Hu,C.H. (2020) Epigenetic regulation of mesenchymal stem cell homeostasis. *Trends Cell Biol.*, **30**, 97–116.
89. Wang,T., Kong,S., Tao,M. and Ju,S. (2020) The potential role of RNA N6-methyladenosine in cancer progression. *Mol. Cancer*, **19**, 88.
90. Wanna-Udom,S., Terashima,M., Lyu,H., Ishimura,A., Takino,T., Sakari,M., Tsukahara,T. and Suzuki,T. (2020) The m6A methyltransferase METTL3 contributes to transforming growth factor-beta-induced epithelial-mesenchymal transition of lung cancer cells through the regulation of JUNB. *Biochem. Biophys. Res. Commun.*, **524**, 150–155.
91. Zhao,M., Sun,J. and Zhao,Z. (2013) TSGene: a web resource for tumor suppressor genes. *Nucleic Acids Res.*, **41**, D970–D976.
92. Zeng,C., Huang,W., Li,Y. and Weng,H. (2020) Roles of METTL3 in cancer: mechanisms and therapeutic targeting. *J. Hematol. Oncol.*, **13**, 117.
93. Jaud,M., Philippe,C., Di Bella,D., Tang,W., Pyronnet,S., Laurell,H., Mazzolini,L., Rouault-Pierre,K. and Touriol,C. (2020) Translational regulations in response to endoplasmic reticulum stress in cancers. *Cells*, **9**, 540.
94. Zhang,H., Shi,X., Huang,T., Zhao,X., Chen,W., Gu,N. and Zhang,R. (2020) Dynamic landscape and evolution of m6A methylation in human. *Nucleic Acids Res.*, **48**, 6251–6264.
95. Croft,D., O'Kelly,G., Wu,G., Haw,R., Gillespie,M., Matthews,L., Caudy,M., Garapati,P., Gopinath,G., Jassal,B. *et al.* (2011) Reactome: a database of reactions, pathways and biological processes. *Nucleic Acids Res.*, **39**, D691–D697.
96. Wang,C.X., Cui,G.S., Liu,X., Xu,K., Wang,M., Zhang,X.X., Jiang,L.Y., Li,A., Yang,Y., Lai,W.Y. *et al.* (2018) METTL3-mediated m6A modification is required for cerebellar development. *PLoS Biol.*, **16**, e2004880.
97. Widagdo,J. and Anggono,V. (2018) The m6A-epitranscriptomic signature in neurobiology: from neurodevelopment to brain plasticity. *J. Neurochem.*, **147**, 137–152.
98. Zheng,Q., Hou,J., Zhou,Y., Li,Z. and Cao,X. (2017) The RNA helicase DDX46 inhibits innate immunity by entrapping m(6)A-demethylated antiviral transcripts in the nucleus. *Nat. Immunol.*, **18**, 1094–1103.
99. Winkler,R., Gillis,E., Lasman,L., Safra,M., Geula,S., Soyris,C., Nachshon,A., Tai-Schmiedel,J., Friedman,N., Le-Trilling,V.T.K. *et al.* (2019) m(6)A modification controls the innate immune response to infection by targeting type I interferons. *Nat. Immunol.*, **20**, 173–182.
100. Ye,F. (2017) RNA N(6)-adenosine methylation (m(6)A) steers epitranscriptomic control of herpesvirus replication. *Inflamm. Cell Signal*, **4**, e1604.
101. Tan,B. and Gao,S.J. (2018) RNA epitranscriptomics: Regulation of infection of RNA and DNA viruses by N(6) -methyladenosine (m(6) A). *Rev. Med. Virol.*, **28**, e1983.
102. Li,H.B., Tong,J., Zhu,S., Batista,P.J., Duffy,E.E., Zhao,J., Bailis,W., Cao,G., Kroehling,L., Chen,Y. *et al.* (2017) m(6)A mRNA methylation controls T cell homeostasis by targeting the IL-7/STAT5/SOCS pathways. *Nature*, **548**, 338–342.
103. Feng,Z., Li,Q., Meng,R., Yi,B. and Xu,Q. (2018) METTL3 regulates alternative splicing of MyD88 upon the lipopolysaccharide-induced inflammatory response in human dental pulp cells. *J. Cell. Mol. Med.*, **22**, 2558–2568.
104. Agace,W.W. and McCoy,K.D. (2017) Regionalized development and maintenance of the intestinal adaptive immune landscape. *Immunity*, **46**, 532–548.
105. Holtorf,A., Conrad,A., Holzmann,B. and Janssen,K.P. (2018) Cell-type specific MyD88 signaling is required for intestinal tumor initiation and progression to malignancy. *Oncoimmunology*, **7**, e1466770.
106. Moresco,E.M., LaVine,D. and Beutler,B. (2011) Toll-like receptors. *Curr. Biol.*, **21**, R488–R493.
107. Sledz,P. and Jinek,M. (2016) Structural insights into the molecular mechanism of the m(6)A writer complex. *Elife*, **5**, e18434.
108. Wang,P., Doxtader,K.A. and Nam,Y. (2016) Structural basis for cooperative function of Mettl3 and Mettl14 methyltransferases. *Mol. Cell*, **63**, 306–317.
109. Wang,X., Feng,J., Xue,Y., Guan,Z., Zhang,D., Liu,Z., Gong,Z., Wang,Q., Huang,J., Tang,C. *et al.* (2016) Structural basis of N(6)-adenosine methylation by the METTL3-METTL14 complex. *Nature*, **534**, 575–578.
110. Jiang,L., Chen,T., Xiong,L., Xu,J.H., Gong,A.Y., Dai,B., Wu,G., Zhu,K., Lu,E., Mathy,N.W. *et al.* (2020) Knockdown of m6A methyltransferase METTL3 in gastric cancer cells results in suppression of cell proliferation. *Oncol. Lett.*, **20**, 2191–2198.
111. Wu,Z., Shi,Y., Lu,M., Song,M., Yu,Z., Wang,J., Wang,S., Ren,J., Yang,Y.G., Liu,G.H. *et al.* (2020) METTL3 counteracts premature aging via m6A-dependent stabilization of MIS12 mRNA. *Nucleic Acids Res.*, **48**, 11083–11096.
112. Xu,J., Chen,Q., Tian,K., Liang,R., Chen,T., Gong,A., Mathy,N.W., Yu,T. and Chen,X. (2020) m6A methyltransferase METTL3 maintains colon cancer tumorigenicity by suppressing SOCS2 to promote cell proliferation. *Oncol. Rep.*, **44**, 973–986.
113. Lin,Z., Hsu,P.J., Xing,X., Fang,J., Lu,Z., Zou,Q., Zhang,K.J., Zhang,X., Zhou,Y., Zhang,T. *et al.* (2017) Mettl3-/Mettl14-mediated mRNA N(6)-methyladenosine modulates murine spermatogenesis. *Cell Res.*, **27**, 1216–1230.
114. Shi,H., Wei,J. and He,C. (2019) Where, when, and how: context-dependent functions of RNA methylation writers, readers, and erasers. *Mol. Cell*, **74**, 640–650.
115. Li,Y., Xia,L., Tan,K., Ye,X., Zuo,Z., Li,M., Xiao,R., Wang,Z., Liu,X., Deng,M. *et al.* (2020) N(6)-Methyladenosine co-transcriptionally directs the demethylation of histone H3K9me2. *Nat. Genet.*, **52**, 870–877.
116. Huang,H., Weng,H., Zhou,K., Wu,T., Zhao,B.S., Sun,M., Chen,Z., Deng,X., Xiao,G., Auer,F. *et al.* (2019) Histone H3 trimethylation at lysine 36 guides m(6)A RNA modification co-transcriptionally. *Nature*, **567**, 414–419.